Gondwana Research 149 (2026) 314–336

Contents lists available at ScienceDirect

Gondwana Research

journal homepage: www.elsevier.com/locate/gr

New insights on active geodynamics of Iberia and Northwestern Africa from seismic stress and geodetic strain-rate fields

Asier Madarieta-Txurruka [a,b,*], Juan F. Prieto [c], Joaquín Escayo [c], Federico Pietrolungo [d,e,f], José A. Peláez [g], Jesús Galindo-Zaldívar [h,i], Jesús Henares [j], Federica Sparacino [k], Gemma Ercilla [l], José Fernández [m], Mimmo Palano [b,k,n]

[a] Departamento de Geología, Universidad del País Vasco/Euskal Herriko Unibertsitatea (UPV/EHU), Barrio Sarriena s/n, 48940 Leioa, Spain
[b] Dipartimento di Scienze della Terra e del Mare, Università degli Studi di Palermo, Via Archirafi 22, 90123 Palermo, Italy
[c] ETS de Ingenieros en Topografía, Geodesia y Cartografía, Universidad Politecnica de Madrid 28031 Madrid, Spain
[d] Istituto Nazionale di Geofisica e Vulcanologia, Osservatorio Nazionale Terremoti, Via di Vigna Murata 605, 00143 Roma, Italy
[e] Dipartimento di Scienze, Università degli Studi "G. d'Annunzio", Via dei Vestini 31, 66100 Chieti, Italy
[f] Centro inteRUniversitario per l'analisi Sismotettonica Tridimensionale (CRUST), 66100 Chieti, Italy
[g] Departamento de Física, Universidad de Jaén, Campus Las Lagunillas, 23071 Jaén, Spain
[h] Departamento de Geodinámica, Universidad de Granada, Calle Fuentenueva s/n, 18071 Granada, Spain
[i] Instituto Andaluz de Ciencias de la Tierra (IACT), Universidad de Granada, Calle Fuentenueva s/n, 18071 Granada, Spain
[j] Universidad Internacional de La Rioja, Av. de la Paz, 137, 26006 Logroño, Spain
[k] Istituto Nazionale di Geofisica e Vulcanologia, Osservatorio Etneo - Sezione di Catania, Piazza Roma 2, 95125 Catania, Italy
[l] Continental Margins Group, Instituto de Ciencias del Mar (CSIC), Pg. Marítim de la Barceloneta, 37, 08003 Barcelona, Spain,
[m] Instituto de Geociencias (CSIC, UCM). Calle del Doctor Severo Ochoa 7, Ciudad Universitaria, 28040 Madrid, Spain
[n] Istituto di Geologia Ambientale e Geoingegneria, Consiglio Nazionale delle Ricerche (CNR-IGAG), P.le A. Moro, 5, 00185 Rome, Italy

ARTICLE INFO

Keywords:
GNSS velocity field
Geodetic strain-rate field
Seismic stress field
Iberia
Eurasia-Africa plate boundary

ABSTRACT

The convergence between Eurasia and Africa during Alpine orogeny drives complex geodynamic processes, involving multiple crustal blocks. In the Atlantic-Mediterranean transition zone, the geodynamics is controlled by the two main plates, the former Iberian microplate and the Alboran Domain. Nowadays, these crustal domains, composed of continental and oceanic crust of varying ages, show distinct deformation behaviors under the current regional stress regime. Through analysis of an enhanced earthquake focal mechanism catalog and updated GNSS velocity field, we constrained the crustal stress–strain fields with unprecedented resolution. Three key findings emerged. First, the different crustal blocks interacting in the region determine the stress–strain fields along the plate boundary, allowing us to define four sectors: Atlantic, Gibraltar, Alboran, and Algero-Balearic. Second, in the Atlantic sector, stresses are directly transferred between Africa and Eurasia, while westward they are absorbed by the thinned continental crust of the Alboran Domain and the continental margins of the Gibraltar Arc and Tell Cordillera. This framework, combined with the oblique Eurasia-Africa convergence relative to the Southwestern Iberian margin, could facilitate the clockwise rotation of Iberia. Finally, intraplate regions with low horizontal strain-rates still show tectonic activity influenced by regional compression and other geodynamic processes driven by vertical stresses. This study highlights the value of combined grid-based stress and strain-rate field analysis for understanding geodynamic processes in complex plate boundary regions.

1. Introduction

The Alpine Orogeny resulted from the closure of the Tethys Ocean (e.g., Schmid et al., 2004) due to counterclockwise convergence of the African plate relative to the Eurasian one (e.g., van Hinsbergen et al., 2014). Beyond the interaction of the Eurasian and African plates, other microplates, as well as smaller crustal blocks (e.g., Bouillin et al., 1986), played a significant tectonic role (Fig. 1). The interplay between these continental blocks gave rise to various geodynamic processes that shaped the evolution of the Mediterranean region including rifting and post-

* Corresponding author at: Departamento de Geología, Universidad del País Vasco/Euskal Herriko Unibertsitatea (UPV/EHU), Barrio Sarriena s/n, 48940 Leioa, Spain.
E-mail address: asier.madarieta@ehu.eus (A. Madarieta-Txurruka).

https://doi.org/10.1016/j.gr.2025.08.020
Received 9 April 2025; Received in revised form 25 June 2025; Accepted 22 August 2025
Available online 18 September 2025

rift thermal subsidence (Maillard and Mauffret, 1999), inversion of rifted margins (Martínez-García et al., 2013), subduction and back-arc extension (Jolivet and Faccenna, 2000), continental collision (Vissers and Meijer, 2012), and syn/post orogenic collapse (Jolivet and Faccenna, 2000), among others.

In the Mediterranean-Atlantic transition zone, the Alpine Orogeny is determined by the former Iberian microplate (Fig. 1). The spatial and temporal distribution of Cenozoic deformation led to complex evolutionary timelines across Iberian margins and Northwestern Africa, giving rise to orogens shaped by diverse processes at different stages of tectonic development: a) Oligocene-Miocene collision between Iberia and Eurasia, resulting in the formation of the Pyrenean-Cantabrian Cordillera (e.g., Teixell et al., 2018), b) inversion of the thinned continental crust in internal zones of Iberia and Northwestern Africa since the Oligocene (de Vicente et al., 2009; Teixell et al., 2005), c) Miocene rifting along Eastern Iberia and opening of the Valencia Trough (Roca and Guimerà, 1992), d) a continuous collision since the Miocene of the ALKAPECA domains with continental margins of Iberia and Northwestern Africa, developing the Gibraltar Arc and the Tell Cordillera, respectively (Rosenbaum et al., 2002; Romagny et al., 2020), e) related back arc extension leading to the formation of thinned continental crust in the Alboran Sea and oceanic crust in the Algero-Balearic Basin (Jolivet et al., 2008; Gómez de la Peña et al., 2018), and f) active thrusting between Atlantic oceanic crust of Africa and Eurasia (e.g., Tortella et al., 1997; Martínez-Loriente et al., 2013).

This complex interaction, determining the stresses in each region, makes the Atlantic-Mediterranean transition zone an extraordinary laboratory for studying the current geodynamics of the continental and oceanic crucial blocks involved. Strain, on the other hand, is the result of the stress acting across the crust. Typically, there is always a direct geometric relationship between the two. In the case of isotropic homogeneous elastic materials, if the stress and strain-rate fields are expressions of the same process, they are observed to be parallel (e.g., Townend and Zoback, 2006). However, in anisotropic and inhomogeneous materials, such as a heterogeneously deformed crust, and in simple shear zones, the relationship between stress and strain can become oblique (e.g., Zoback et al., 1987; Lachenbruch and Sass, 1992; Flesch et al., 2000; Palano, 2015). Determining stress through earthquake focal mechanism solutions (FMSs) provides insights into the stress released during seismic events (Aki and Richards, 2002). In contrast,

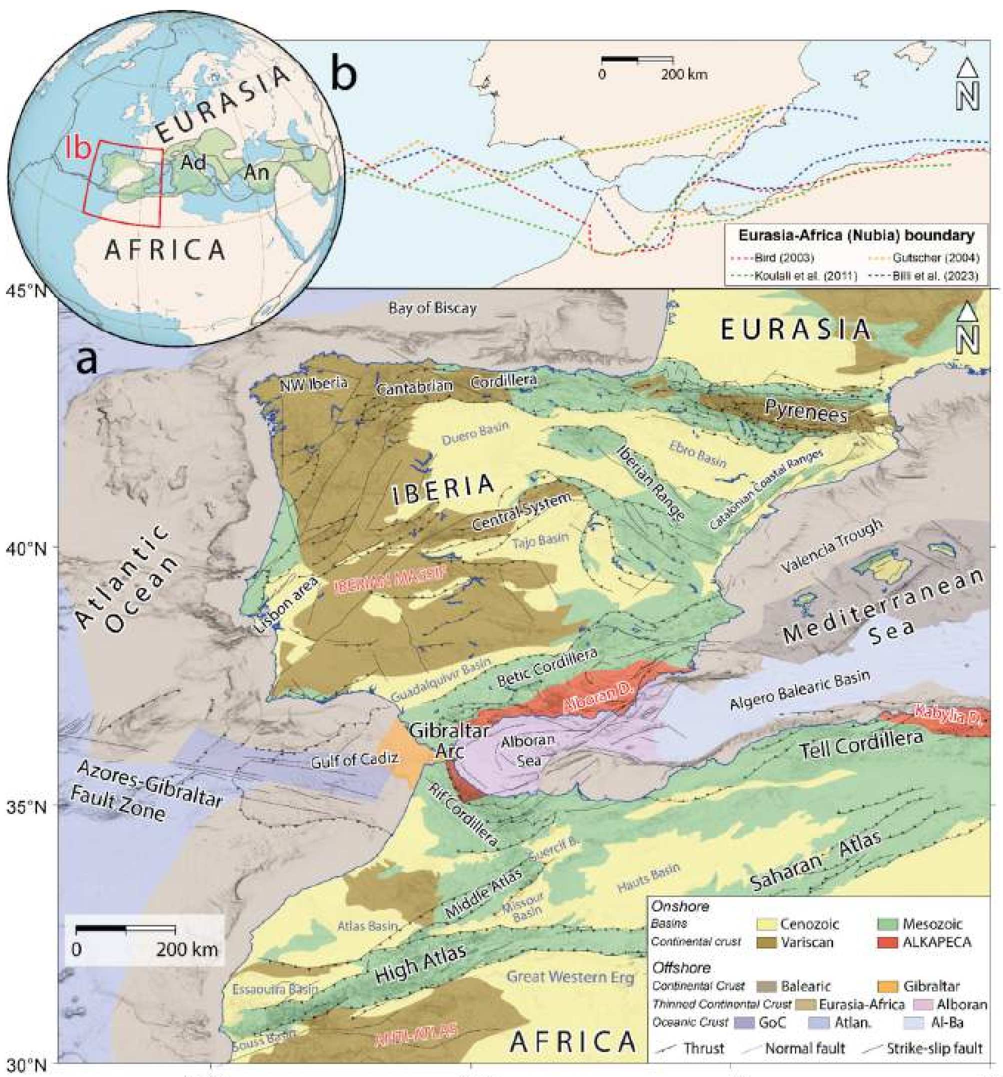

Fig. 1. Geological context. a) Simplified geological map modified from Rodríguez-Fernández et al. (2015) and Palano et al. (2015) in Iberia and from Anahnah et al. (2011) in Northwestern Africa. The offshore area is modified from Druet et al. (2023). GoC: Gulf of Cadiz. Al-Ba: Algero-Balearic b) Eurasia-Africa plate boundary from Bird (2003), Gutscher (2004), Koulali et al. (2011) and Billi et al. (2023). Inset: Global map with the location of the study area at the westernmost end of the Alpine orogenic belt (highlighted in green). Ib: Iberia, Ad: Adria, An: Anatolia. (For interpretation of the references to color in this figure legend, the reader is referred to the web version of this article.)

strain estimates derived from regional dense GNSS networks capture shallow crustal deformation resulting from stress, that may be released either seismically or aseismically (e.g., Kreemer et al., 2014). By integrating and comparing these two approaches, it is possible to achieve a more comprehensive understanding of tectonic and geodynamic processes, as applied in other regions worldwide, such as Southern Africa (Bird et al., 2006), Japan (Townend and Zoback, 2006), Italy (Palano, 2015; Palano et al., 2011), western North America (e.g., Balfour et al., 2011), Dead Sea Fault System (Palano et al., 2013a), the Himalaya-Tibet region (e.g., Pietrolungo et al., 2024), the southwest Iceland (Keiding et al., 2009) and the Pannonian region (Porkoláb et al., 2025).

In this study we aim to provide new insights on how crustal stress and surface strain are related along both the diffuse Eurasia-Africa plate boundary in the westernmost Mediterranean region and the internal regions of Iberia and Northwestern Africa. To achieve this, a comprehensive compilation of all available earthquake focal mechanism solutions (FMSs) has been performed to estimate the crustal stress field affecting the region. Additionally, a new velocity field as well as the corresponding strain-rate field have been computed.

2. Background setting

2.1. Geodynamic setting

The Alpine geodynamic evolution of westernmost Mediterranean began during the Permo-Triasssic rifting of Pangea which thinned the Variscan lithosphere, delineating the future margins of the Iberian microplate and the rifted margins within Iberia and Northwestern Africa (Arche and López-Gómez, 1996; Angrand et al., 2020). The resulting rifted zones facilitated the breakup of the lithosphere during the Jurassic-Cretaceous extensional phase. The northward migration of the central Atlantic rifting during the early-middle Jurassic separated Eurasia, Iberia, and Africa from North America, opening the Atlantic Ocean. The extension localized also in Northwestern Africa forming rifted basins (e.g., Jacobshagen et al., 1988) and along the actual Southern Iberian and the Northern African margins, forming the Ligurian-Tethys basins (Schettino and Turco, 2011; Pedrera et al., 2020). In the late Jurassic, the central Atlantic rifting evolved northward and later eastward opening the Bay of Biscay and Pyrenean Basin between the Northern Iberian margin and Eurasia (Thinon et al., 2003; Pedrera et al, 2021, 2023). The internal part of Iberia underwent extension, leading to the formation of the Mesozoic Iberian Basin (e.g., Aurell et al., 2019) (Fig. 1). The opening of the margins continued till the late Cretaceous, when African plate began to push northward, modifying the motion of Iberia (e.g., Srivastava et al., 1990).

During the Cenozoic, the central Atlantic continued opening, and the Western Iberian margin remained almost undeformed. However, mainland Iberia and the other margins have been inverted due to the Eurasia-Africa convergence (e.g., Vergés and Fernàndez, 2006). The Alpine Orogeny started in the Northern Iberian margin. During the late Cretaceous-middle Miocene, the Pyrenean Basin and the southern margin of the Bay of Biscay were inverted, resulting in the Pyrenean Cordillera and Cantabrian Mountains, respectively (Teixell et al., 2018; Pedrera et al., 2023) (Fig. 1). The Iberian Massif and the Mesozoic Iberian Basin were also deformed during the late Eocene-early Miocene, leading to the formation of the Central System and the Iberian Range (de Vicente et al., 2009, 2018). Meanwhile, Africa continued its northwestward motion, inverting the preexisting rift basins and leading to the formation of the Middle Atlas, High Atlas and Saharan Atlas (Fig. 1). During the Miocene, eastern Iberia underwent extension during the opening of Valencia Trough (Roca and Guimerà, 1992), driven by subduction with rollback of the Tethys Ocean (Fang et al., 2021).

Since middle Miocene, the Northern Iberian margins have remained almost stable while the convergence was mainly concentrated in the Southern Iberian and Northwestern African margins (Fig. 1). The subduction with rollback of the Tethys below Eurasia, that previously led to the formation of the Valencia Trough, displaced ALKAPECA domain –formed by Alboran, Kabylia, Peloritani and Calabria– towards the south. Peloritani and Calabria moved toward the southeast and now belong to the Calabrian subduction system (Chiarabba and Palano, 2017). Kabylia Domain collide with Africa developing the Tell Cordillera (Mauffret, 2007; van Hinsbergen et al., 2014). The Alboran Domain, on the opposite, shifted to southwest colliding with the Southeastern Iberian and Northwestern African margins. During this process, the Gibraltar Arc was developed, formed by the Betic Cordillera in Iberia and Rif Cordillera in Africa (Rosenbaum et al., 2002; Romagny et al., 2020). A back-arc extension related to this phase resulted in accretion of the Algero-Balearic oceanic crust and pronounced thinning of the continental crust throughout the Alboran Basin (Jolivet et al., 2008; Gómez de la Peña et al., 2018). During this period the development of Atlas Cordillera continues (Teixell et al., 2005; Chalouan et al., 2023).

Currently, the continuous NW-SE convergence between Eurasia and Africa produces a *trans*-pressive boundary along the Azores-Gibraltar Fault System (Buforn et al., 1988; Custódio et al., 2015), indentation along the Alboran Sea and Southeastern Iberian margin (Galindo-Zaldívar et al., 2018; Estrada et al., 2018; Tendero-Salmerón et al., 2024), and compression along the Tell Cordillera (e.g., Frizon de Lamotte et al., 2000), defining the actual diffuse plate boundary (e.g., Gómez de la Peña et al., 2022; Billi et al., 2023) (Fig. 1b).

2.2. Active faults

Ongoing geodynamic processes control the crustal stress and the localization of active tectonic structures that currently shape the region. Active faults facilitate the displacement of crustal blocks and determine strain patterns. Over the past decades, extensive research has led to the identification and characterization of numerous active faults. Fig. 2 illustrates the active faults, color-coded according to their kinematics, compiled from the Quaternary Fault Database of Iberia (QAFI) (García-Mayordomo and Martín-Banda, 2022), and the GEM Global Active Faults database (Styron and Pagani, 2020) for Northwestern Africa (Supplementary File S1). Faults classified as active in the QAFI database are shown with solid lines, while those "debated faults" are represented by dashed lines. In this study, the latter are considered potentially active.

Active faults are mainly concentrated in the Eurasian-African plate boundary and in the Atlas and Pyrenean cordilleras (Fig. 2). The Atlantic sector of the Eurasian-African plate boundary is formed by the Azores-Gibraltar fracture zone (Laughton and Whitmarsh, 1974; Jiménez-Munt et al., 2001). It represents a dextral to reverse plate boundary forming *trans*-pressive positive flower structures (Zitellini et al., 2009). Between the Atlantic sector of the plate boundary and SW Iberia, the main active structures are NNE-SSW to ENE-WSW striking reverse to reverse sinistral faults (e.g., Martínez-Loriente et al., 2013, 2014, 2018).

Active faults along the Gibraltar Arc are characterized by reverse, strike-slip, and normal faulting kinematics. In the western Betic Cordillera, no major faults are considered active. However, continuous seismicity and GNSS data suggest that an ENE-WSW to NE-SW striking basal thrust could be active (Ruiz-Constán et al., 2009; González-Castillo et al., 2015a). The western Rif Cordillera is also characterized by active thrusts striking NW-SE to E-W (e.g., Koulali et al., 2011). The central Betic Cordillera is primarily characterized by NW-SE to E-W normal faulting (Sanz de Galdeano et al., 2012; Madarieta-Txurruka et al., 2021, 2022; Martín-Rojas et al., 2023). The eastern Rif Cordillera, the Alboran Sea, and the eastern Betic Cordillera are deformed by the active Trans-Alboran Shear Zone (TASZ) and the Eastern Betic shear zone (EBSZ) (e.g., Coppier et al., 1989; Silva et al., 1993; Henares et al., 2024), a NE-SW striking corridor mainly formed by sinistral strike-slip and reverse faults (Booth-Rea et al., 2004; Estrada et al., 2018).

In the Tell Cordillera, the main active faults are E-W to ENE-WSW reverse faults, cut by WNW-ESE dextral-reverse faults (Meghraoui, 1991; Mauffret, 2007). ENE-WSW trending thrust faults are also present

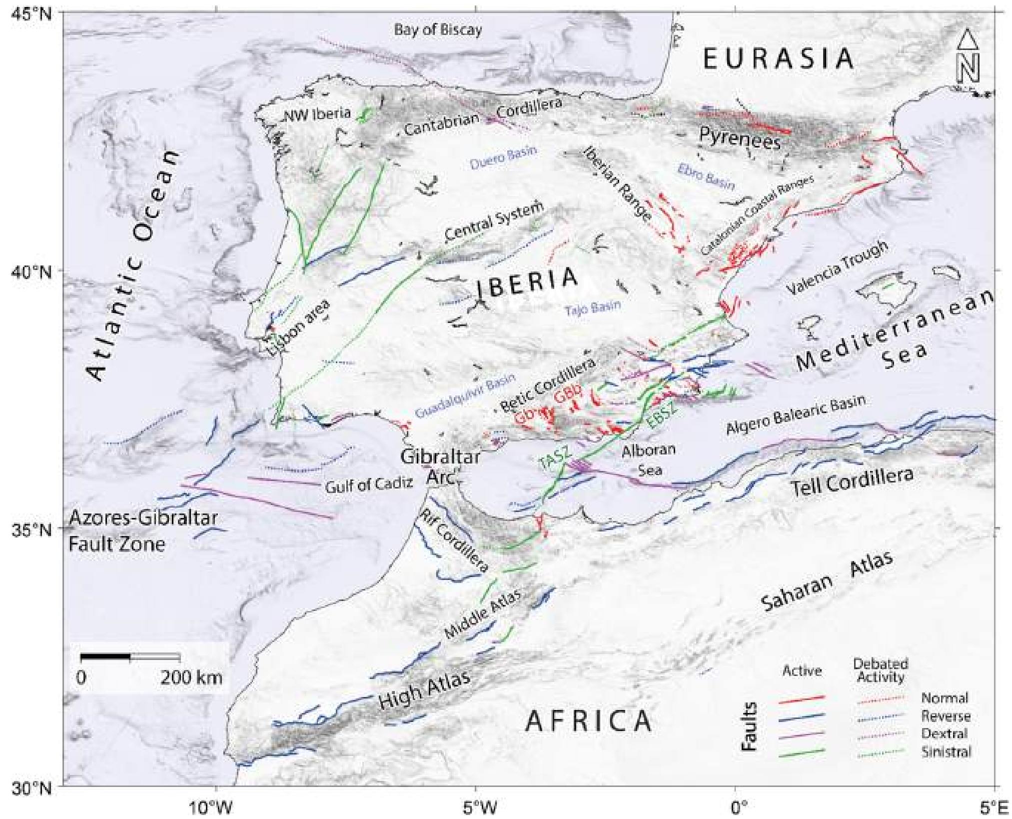

Fig. 2. Recognized active and potentially active faults, color-coded according to the kinematics from the QAFI (García-Mayordomo and Martín-Banda, 2022) and GEM (Styron and Pagani, 2020) databases. TASZ: Trans-Alboran Shear Zone. EBSZ: Eastern Betic Shear Zone Gb: Granada Basin. GBb: Guadix-Baza Basin.

in the High Atlas (Arboleya et al., 2004), and sinistral to reverse faults in the Middle Atlas (Gomez et al., 1996).

The Pyrenees, the Iberian Range, and the NW coast of Iberia are dominated by active normal faulting, mostly parallel to the mountain ranges. In the Pyrenees, the faults strike E-W (Lacan and Ortuño Candela, 2012), in the Iberian Range are oriented NW-SE to N-S (e.g., Peiro, 2023), while in the Catalonia Coastal Ranges strike NE-SW (Perea et al., 2012). Finally, western Iberia is mainly affected by large NNE-SSW sinistral and NE-SW reverse faults (Villamor et al., 2012; Cabral, 2012) but also, by NW-SE dextral faults in the Cantabrian Mountains (López-Fernández et al., 2018; Fernández-Viejo et al., 2021; Martín-González et al., 2023).

2.3. Seismicity

In the last millennium the study region has been affected by several earthquakes with moment magnitude Mw > 6 mainly located along the Eurasia-Africa plate boundary (Peláez et al., 2007; Hamdache et al., 2010; Grünthal and Wahlström, 2012; Stucchi et al., 2013) (Fig. 3 and Table S1). The main historical earthquake close to Iberia was the Mw 8.7, 1755 Lisbon earthquake (Martínez-Solares et al., 1979; Baptista et al., 1998), occurred between SW Iberia and the Azores-Gibraltar Fault Zone. In this region, four other historical earthquakes with Mw ≥ 7 occurred (CE 1309, 1724, 1816, 1858). Other earthquakes with Mw ≥ 7 also occurred in the Tell Cordillera (CE 1365, 1716, 1825, 1867, 1891 and 1922). Earthquakes with Mw 6–6.9 are more widespread, and they also occur onshore near Lisbon (e.g., CE 1531), Pyrenees (e.g., CE 1428), Gulf of Cadiz (e.g., CE 1722, 1773), Betic Cordillera (e.g., CE 1522, 1680, 1829, 1884), Alboran Sea (e.g., CE 1804), Rif Cordillera (e.g., CE 1624), and westernmost High Atlas (e.g., CE 1731).

The instrumental seismicity recorded by the Spanish Instituto Geográfico Nacional (IGN, 2025) is mainly distributed along the Eurasia-Africa plate boundary, delineating a diffuse contact from the Azores-Gibraltar Fault Zone to the Tell Cordillera, but also in the Pyrenees, High and Middle Atlas, NW Iberia and other Iberian intraplate regions (Fig. 3). Along the Azores-Gibraltar Fault Zone the seismicity is concentrated along NE-SW striking clusters reaching the Southwestern Iberian margin. Most of the seismicity is above 50 km depth and the maximum recorded magnitude is related to the Mw 7.9, February 1969 earthquake. The seismicity in SW Iberia and adjacent Western Iberian margin is more widespread, also reaches 50 km and magnitude hardly exceed Mw 5.0. Earthquake focal mechanism solutions (FMSs) along these regions suggest main reverse and strike-slip faulting (e.g., Buforn et al., 1988; Stich et al., 2007; Custódio et al., 2015).

The Gibraltar Arc is affected by a crustal seismicity mainly concentrated in the Betic Cordillera, eastern Rif Cordillera and the Alboran Sea. The maximum magnitude reached Mw 6.3 during the 2016 series in the Alboran Sea (Hamdache et al., 2022). Along the Betic Cordillera only a few earthquakes exceeded Mw 5.0. Available FMSs suggest reverse and strike-slip faulting in the western Betic Cordillera (Ruiz-Constán et al., 2009), mainly normal faulting in the central Betic Cordillera (Madarieta-Txurruka et al., 2021, 2022), strike-slip faulting along a NE-SW band from the eastern Rif Cordillera to the eastern Betic Cordillera crossing the Alboran Sea (Grevemeyer et al., 2015; Galindo-Zaldívar et al., 2018; Henares et al., 2024), and reverse and strike-slip faulting in the western Rif Cordillera. At the internal part of the Gibraltar Arc intermediate seismicity occurs along a N-S sharp arched band reaching 150 km depth. Maximum magnitudes are around Mw 5.0 and FMSs suggest reverse to normal and strike-slip kinematics (Santos-Bueno et al., 2019) (Figs. 3 and S1).

Along the Tell Cordillera, seismicity is widespread concentrated in the shallower 30 km (Hamdache et al., 2010). However, seismicity increases in some clusters located close to the Mediterranean coast reaching M = 7 (Bezzeghoud et al., 1995; Hamdache et al., 2004) earthquakes. Seismicity is mainly related to reverse and strike-slip faulting as shown by the FMSs. Along the Moroccan Atlas seismicity is

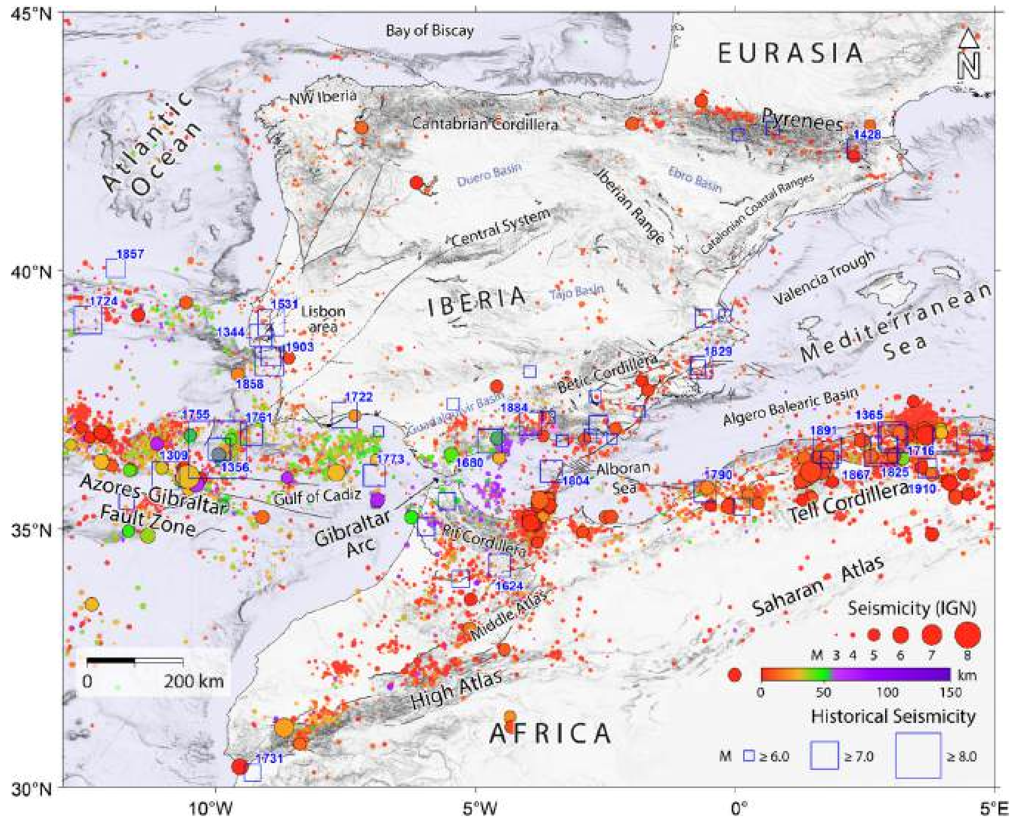

Fig. 3. Historical and instrumental seismicity in Iberia and Northwestern Africa. The historical seismicity (Table S1) comprises all known earthquakes with a macroseismic magnitude exceeding 6.0 that have been documented over the past millennium. Earthquakes with Mw ≥ 6.5 are represented with the year of occurrence. The instrumental seismicity shows earthquakes with M 3.0–4.9 since year 2000 and earthquakes with M > 5.0 since 1960, belonging to the Spanish Instituto Geográfico Nacional database (IGN, 2025). Active and potentially active faults are marked by solid and dashed black lines, respectively.

less frequent. Two clusters highlight in the western and central High Atlas. Main earthquakes were the M 6.0, 1960 Agadir, earthquake, and the M 6.8, September 2023 earthquake (Peláez, 2023). FMSs suggest thrusting and strike-slip faulting related to the main earthquakes (Udías et al., 1989).

Along the Pyrenees the seismicity involves crustal depths and concentrates mostly in the western half. The magnitude of earthquakes hardly exceeds Mw 5.0. FMSs suggest a dominant normal faulting regime coupled with secondary strike-slip faulting, and some reverse solutions (Rigo et al., 2015; Ruiz et al., 2023). The Northeastern Iberian margin is affected by low magnitude seismicity following the axis of the Catalonian Coastal Ranges, related to strike-slip to normal FMSs. In the internal part of Iberia scarce seismicity occurs, concentrated around the Iberian Range (e.g., Peiro, 2023) with normal and strike-slip FMSs. Finally, in the Northern Iberian margin seismicity is scarce. This region is characterized by low to moderate magnitude crustal seismicity clusters, reaching sporadically M 5.0. The seismicity is mainly related to strike-slip and normal FMSs (Martín-González et al., 2023).

3. Methodology

3.1. Stress field estimation

The slip direction along a fault during an earthquake reflects stress conditions at the source (e.g., Anderson, 1905; Bott, 1959). Consequently, earthquake focal parameters provide valuable insights into the current tectonic stress field within the seismogenic layer (Michael, 1987). For this reason, earthquake focal mechanism solutions (FMSs) are essential and widely used indicators of stress, and their formal inversion enables the determination of the regional crustal stress field (Vavryčuk, 2014).

The FMS dataset compiled here considered mostly available solutions along Iberia and Northwestern Africa, onshore and offshore. An exhaustive compilation has been made considering the following catalogs and publications to increase the coverage of the entire study area:

- ***Global catalogs***: Global Centroid Moment Tensor Catalog (CMT; https://www.globalcmt.org/CMTsearch.html).
- ***European catalogs***: European-Mediterranean Regional Centroid-Moment Tensors Catalog (RCMT; https://rcmt2.bo.ingv.it/), ETH Zürich catalog (ETHZ; Braunmiller et al., 2002).
- ***Iberian catalogs***: Instituto Geográfico Nacional (IGN; https://www.ign.es/web/en/ign/portal/tensor-momento-sismico), Instituto Andaluz de Geofísica (IAG; https://iagpds.ugr.es/investigacion/proyectos/moment-tensor-catalogue).
- ***Compilation catalogs***: International Seismological Centre (ISC; https://www.isc.ac.uk/iscbulletin/search/fmechanisms/), Euro-Mediterranean Seismological Centre (EMSC; https://www.emsc-csem.org/Earthquake_data/tensors.php), Earthquake Mechanisms of the Mediterranean Area (EMMA; Vannucci and Gasperini, 2004), FMHex20 (Mazzotti et al., 2021).
- ***Peer-reviewed articles and other publications*** (See references in Table S2)

In many cases, a seismic event had multiple although similar FMSs proposed by different sources. It was therefore necessary to establish a set of criteria for selecting the solution to use for a given seismic event. Overall, the following criteria were considered: 1) detailed calculation of FMSs from peer-review papers analyzing specific earthquakes or study areas are preferred over solutions from catalogs, giving preference to the most recent publications, 2) waveform inversion solutions are preferred over the one computed by P-waves polarities, and 3) the

Iberian and European catalogs are preferred over global catalogs due to their better coverage of stations and the use of more detailed crustal velocity models. The final catalog comprises ~2200 FMSs from 1910 to 2024 with estimated magnitude in the 2–8 range (Table S2); a plot is shown in Fig. S1. Spatially, most of the FMSs are along the Eurasia-Africa boundary (~80 %), along the Azores-Gibraltar Fault Zone, Gibraltar Arc and Tell Cordillera. A small set of FMs (~10 %) are located along the Pyrenees, while other ones are widespread located along NW Iberia, the Lisbon area and Moroccan Atlas. Regarding the focal depth distribution, most of the FMSs (89 %) are crustal (< 30 km) and are widespread along the active areas quoted before. Solutions with depths of up to 50 km account for 6 % of the data and are predominantly located to the southwest of Iberia, mainly in offshore regions. Solutions with intermediate depth (50–150 km) account for ~5 % and are mainly located in the internal part of the Gibraltar Arc. Finally, five deep earthquake FMSs (>600 km) are located beneath the central Betic Cordillera.

For the inversion of the crustal stress field, FMSs deeper than 50 km and with magnitude below M 3.0 are discarded (in red in Table S2). The remaining ~1400 FMSs (Fig. 4) are inverted using the STRESSINVERSE software developed by Vavryčuk (2014). This software computes the geometry of the three principal stress axes (σ_1, σ_2 and σ_3) and stress ratio R (Eq. (1), by means of an iterative inversion approach considering all the nodal plane combinations till obtaining the combination more susceptible to shear faulting. The confidence limits are estimated by computing the maximum differences between the inversion for noise-free and noisy data with 100 noise realizations, following the methodology of Vavryčuk (2014). The stress ratio (R) indicates the shape of the stress ellipsoid; values of R ≈ 1 correspond to a prolate shape of the ellipsoid (uniaxial compression), values of R ≈ 0.5 to a triaxial shape and values of R ≈ 0 to an oblate shape (uniaxial extension). The inversion is applied along a 0.5° resolution grid and computed with a half-cell overlapping in every cell with a minimum of 8 available FMSs (Fig. 5 and Table S3).

$$R = \frac{\sigma_1 - \sigma_2}{\sigma_1 - \sigma_3} \tag{1}$$

For regional stress analysis, mapping the maximum horizontal compressive stress (σ_{Hmax}) azimuth (e.g., Balfour et al. 2005) helps compare seismological stress directions with geodetic strain-rates (Townend and Zoback, 2006). A practical but simplified approach assumes σ_{Hmax} aligns with the trend of the largest subhorizontal principal stress (σ_1 or σ_2), valid only if one principal stress is strictly vertical. However, this introduces errors depending on the principal stress axes plunge or R. To refine this approach, we adopt the Lund and Townend (2007) methodology, which incorporates both principal stress axes and R to calculate the maximum horizontal stress (σ_{Hmax}) for each grid cell. To increase the coverage of σ_{Hmax} data, the former solutions are combined with σ_{Hmax} indicators from individual earthquake FMSs with M ≥ 4.5, along with other stress indicators obtained from the World Stress Map (Heidbach et al., 2018) (Table S3). Finally, the trajectories of the σ_{Hmax} field (Fig. 5) are estimated.

3.2. GNSS data processing and velocity and strain-rate fields estimation

The GNSS dataset used here includes 530 continuous stations belonging to the EUREF permanent network, SONEL database, Portuguese RENEP and SERVIR networks, Spanish ERGNSS network, French RGP network and other 15 networks developed by regional institutions (Table S4), with time interval of the longest observations covering almost 25 years, from 1999.00 to 2024.00. In addition to continuous GNSS sites, we included data from 25 episodic GNSS sites located in Morocco (Koulali et al., 2011) with surveys spanning the 1999.80–2006.71 time interval, available in the UNAVCO archive (htt

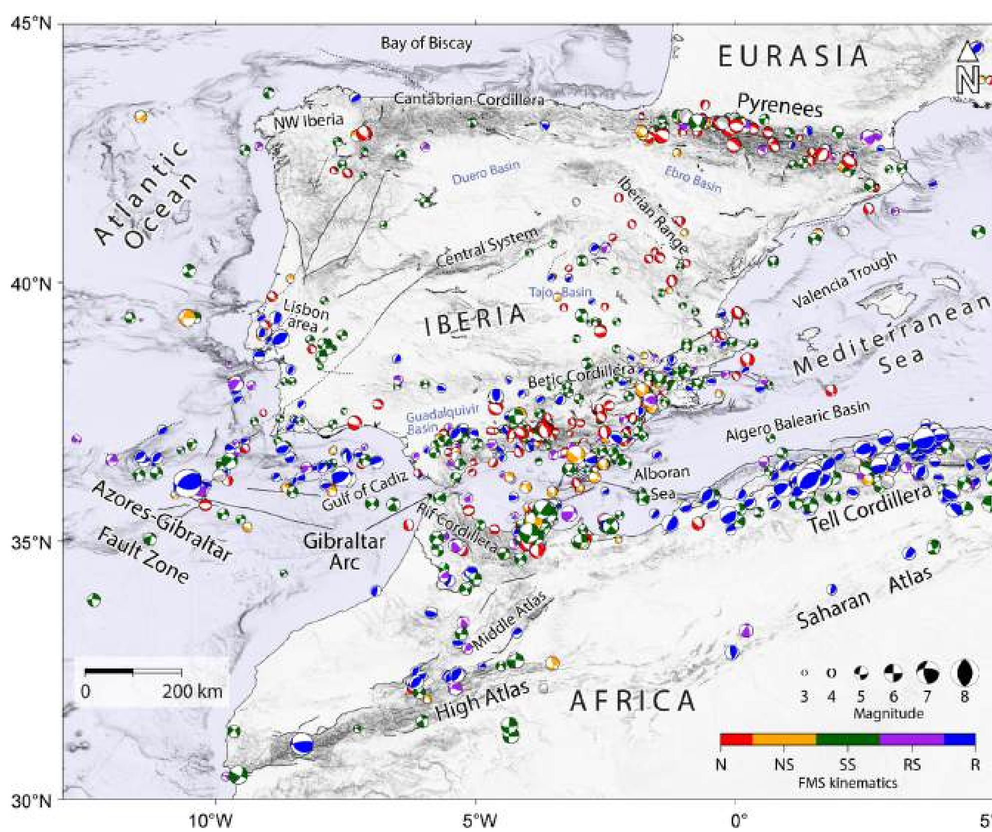

Fig. 4. FMSs in Iberia and Northwestern Africa. The solutions reported here, with a magnitude greater than M 3 and a depth less than 50 km, were used in the stress inversion. FMSs are displayed with compressive quadrants color-coded according to the Frohlich (1992) classification scheme. Active and potentially active faults are marked by solid and dashed black lines, respectively.

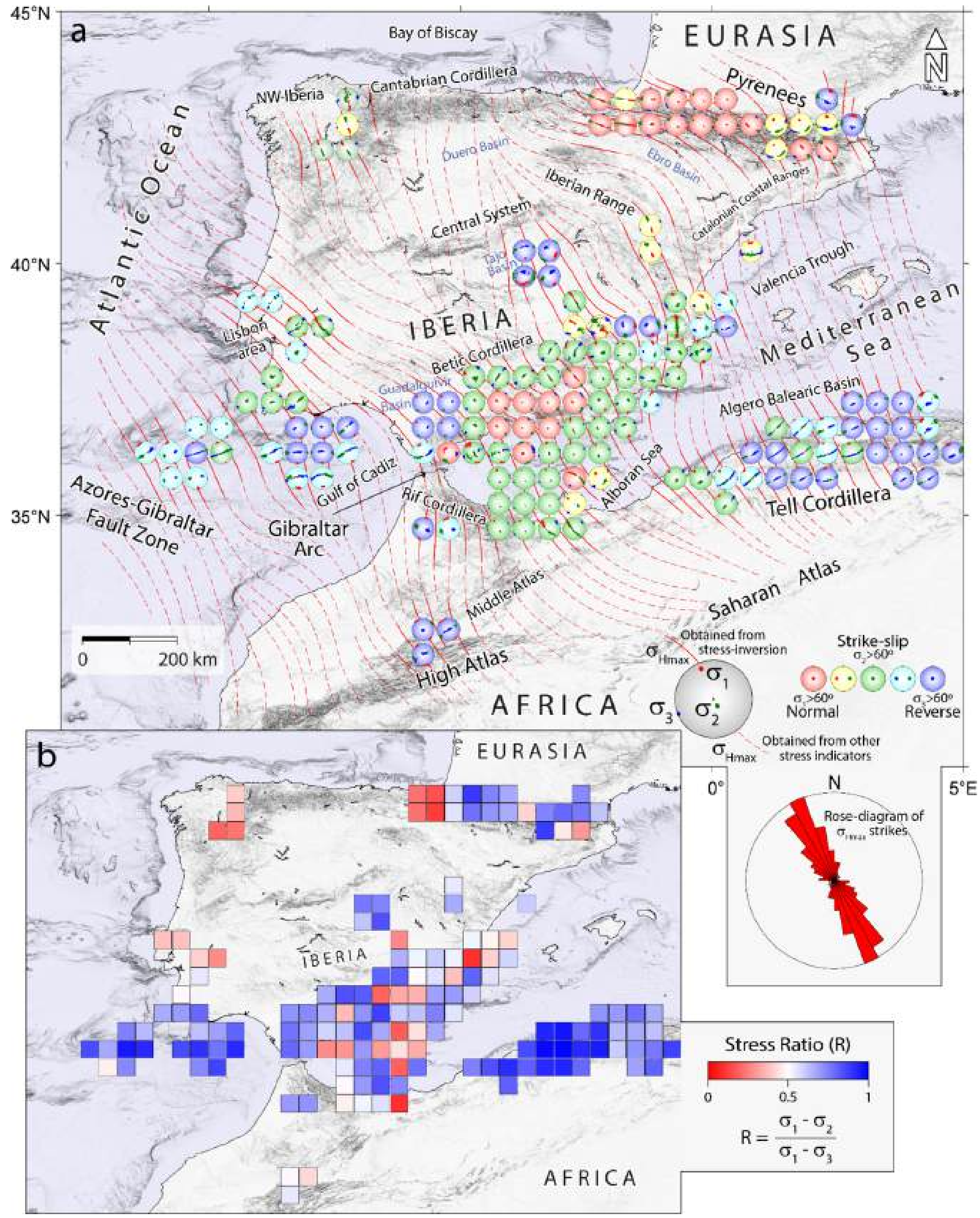

Fig. 5. Computed stress field. a) Stereoplots depict the stress field by representing the principal stress axes (σ_1 in red, σ_2 in green, and σ_3 in blue) and their estimated confidence limits derived from each iterative solution during the inversion process. Stereoplots are color-coded according to the principal stress axis (or axes) located close to the vertical, considering the final solution available in Table S3. Continuous red lines represent σ_{Hmax} trajectories derived from stress inversion results, while dashed lines depict σ_{Hmax} trajectories obtained from complementary stress indicators. Lower-right inset represents the rose-diagram of the σ_{Hmax} strikes. b) The computed stress ratio (R) in each cell. (For interpretation of the references to color in this figure legend, the reader is referred to the web version of this article.)

ps://www.unavco.org). This dataset hardly increases the number of stations and/or time-interval of previous studies in Iberia and Northwestern Africa (Fernandes et al., 2007; Garate et al., 2015; Koulali et al., 2011; Palano et al., 2013b, 2015; Sparacino et al., 2020).

The GNSS data are processed using the GAMIT/GLOBK software (Herring et al., 2017) (www-gpsg.mit.edu) by adopting the strategy described by Palano et al. (2020). By using the GLORG module of GLOBK, all the GAMIT solutions and their full covariance matrices are combined to estimate a consistent set of positions and velocities in the ITRF14 reference frame (Altamimi et al., 2017). To improve the density of the velocity field we aligned velocity fields available in literature (Bougrine et al., 2019; Cabral et al., 2017; Echeverría et al., 2013, 2015; Garate et al., 2015; Rigo et al., 2015) to the ITRF14 solution computed here by applying a Helmert transformation (Table S5). We align the ITRF14 velocities into a fixed Eurasian and African reference frames (Altamimi et al., 2017) to adequately show the crustal deformation pattern over the study area (Fig. 6 and Table S5). Finally, 85 stations exhibiting anomalous velocities were discarded from the velocity solutions due to rates significantly faster than the regional tectonic signal, likely dominated by non-tectonics deformation (in red in Table S5).

The strain-rate field was computed following the method outlined by Shen et al. (2015) considering a total of 647 stations (Fig. 6). First, we interpolate the GNSS velocity field into a 0.5° resolution grid using Voronoi spatial and Gaussian distance weighting, ensuring nodes do not coincide with GNSS station locations. The weighting threshold (Wt) is strongly influenced by the inter-station distances of GNSS velocities and the measurement uncertainties (Shen et al., 2015), therefore, we tested multiple values. Based on these preliminary results, we selected an

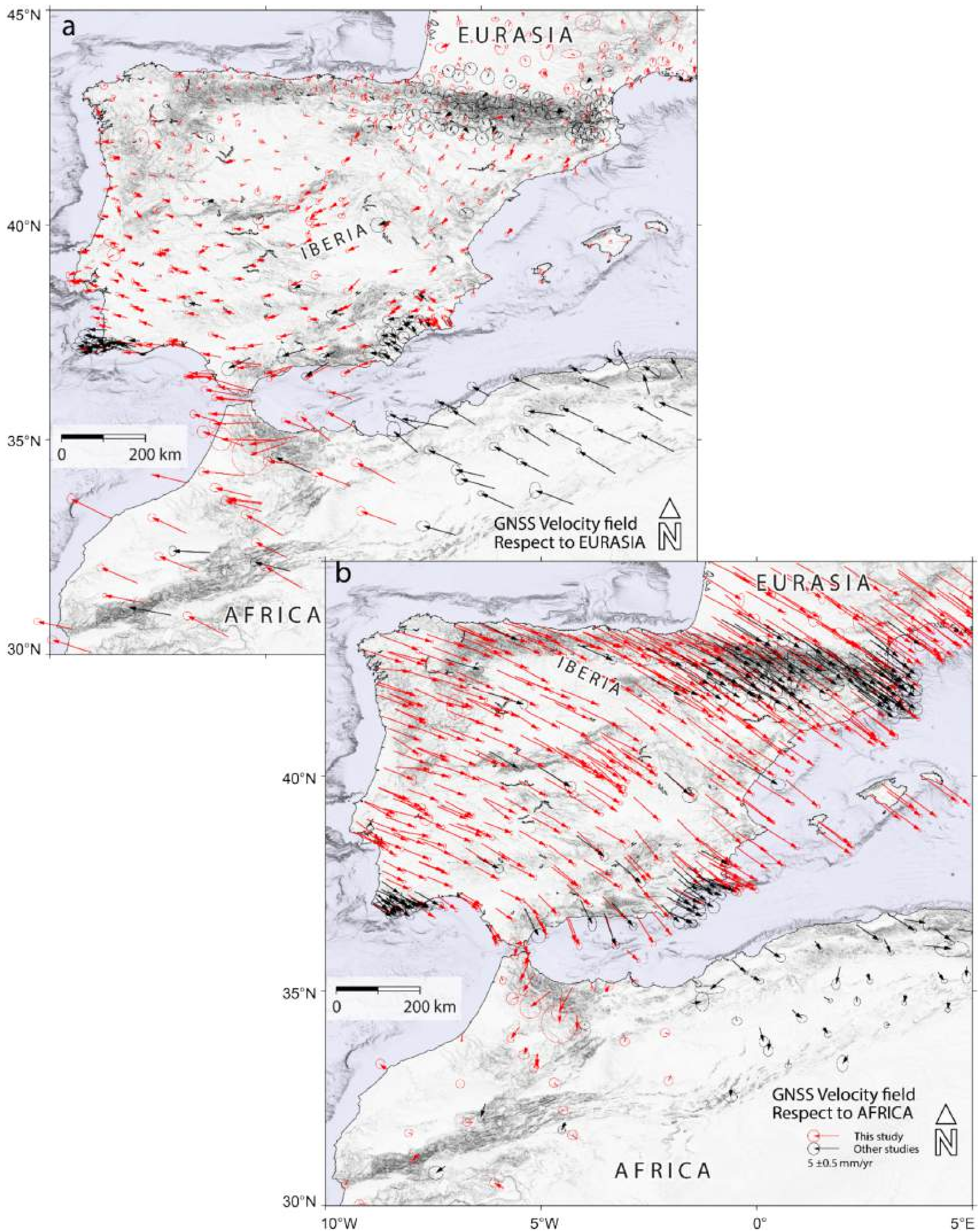

Fig. 6. GNSS-based velocity field. a) GNSS velocities and 95% confidence ellipses in a Eurasia-fixed frame. b) GNSS velocities and 95% confidence ellipses in a Africa-fixed frame.

optimal weighting threshold of 10, which preserves the observed velocity field while ensuring that the model-observed discrepancy exceeds the mean uncertainty of GNSS measurements. Later, the horizontal strain-rate tensor has been computed as the derivative of the velocities. The method of Shen et al. (2015) also provides the areal change and rotational strain-rates. The areal change rate is a useful parameter for characterizing regional crustal kinematics. It quantifies the rate of horizontal surface dilatation (positive values) or contraction (negative values) over time, calculated as the sum of the principal horizontal strain-rates ($\varepsilon_{Hmax} + \varepsilon_{Hmin}$) (Fig. 7). Therefore, this parameter helps to

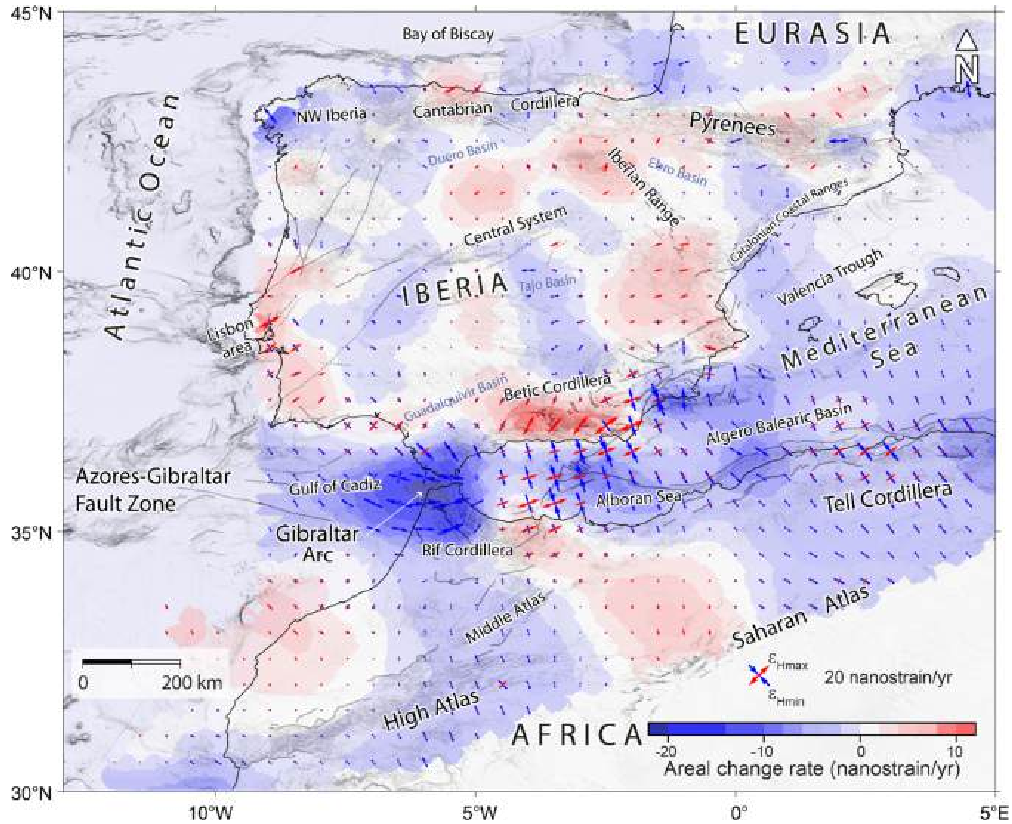

Fig. 7. Computed geodetic strain-rate field. ε_{Hmax} and ε_{Hmin} axes of the strain-rate and areal change rate. Active and potentially active faults are marked by solid and dashed gray lines, respectively.

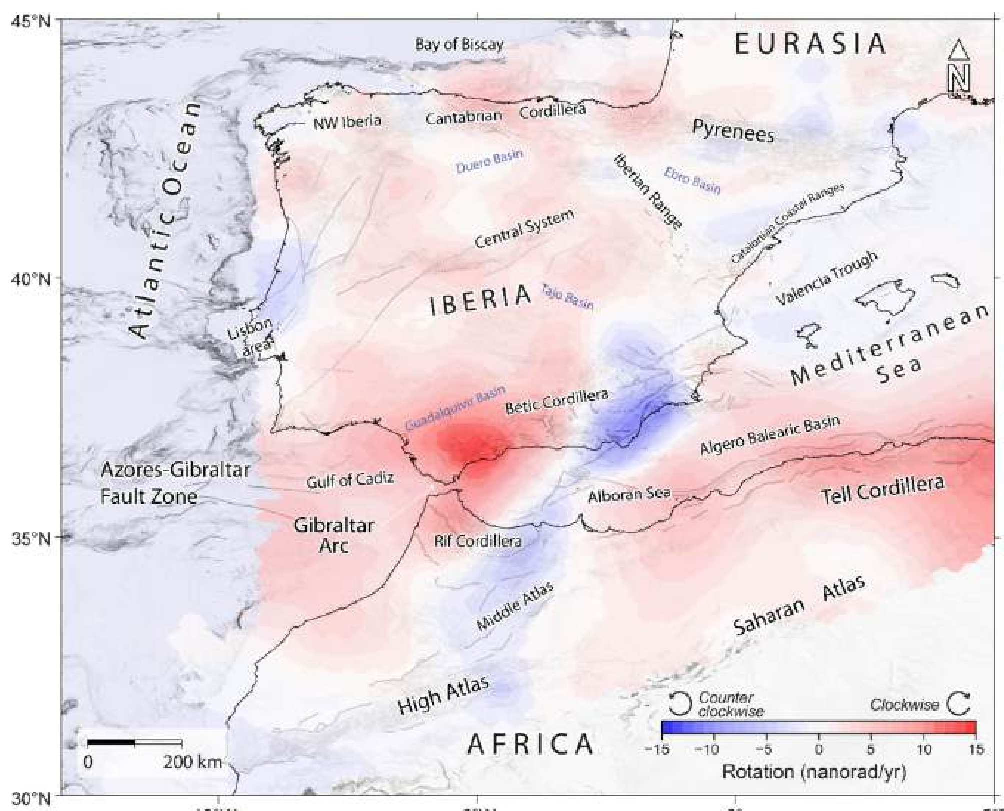

Fig. 8. Rotational strain-rate field. Positives values correspond to clockwise rotation while negative values refer to counterclockwise rotation. Active and potentially active faults are marked by solid and dashed gray lines, respectively.

distinguish between zones of crustal stretching and shortening. Rotational strain-rates quantify the local rotational velocity of crustal blocks due to tectonic deformation (Fig. 8). Moreover, the second invariant was also computed (Eq. (2)), which quantifies the intensity of the deformation on the area (Fig. 9). Finally, the ε_{Hmin} trajectories has been also estimated to achieve an optimal comparison with the σ_{Hmax} (Fig. 9).

$$t_{2inv} = \sqrt{\varepsilon_{xx}^2 + \varepsilon_{yy}^2 + 2\varepsilon_{xy}^2} \quad (2)$$

4. Results

4.1. Stress field

4.1.1. Stress ellipsoids

The stress field (Fig. 5 and Table S3) is depicted through stereoplots representing the principal stress axes derived from each iterative solution during the inversion process (Fig. 5a). Each stereoplot is color-coded according to the principal stress axis (or axes) located close to the vertical, considering the most probable solution available in Table S3. Stress ratio (R) for each computing cell is also shown (Fig. 5b). As previously quoted, the FMSs included in the inversion are predominantly from events within the upper 30 km, none of which exceeding 50 km depth. Therefore, the resulting stress field basically reflects the crustal stress, at least in the 2–30 km depth interval.

Overall, the inversion results are of high quality, as indicated by the low dispersion of iterative solutions in most cells. However, the dispersion is higher in cells where FMSs displayed variable kinematics, particularly in transition zones between different seismotectonic regions, such as the internal part of the Gibraltar Arc. The dispersion increased in regions with a limited number of FMSs such as northwest or central Iberia. In some cells, only the σ_1 axis is well-constrained, while the σ_2 and σ_3 axes partially overlap in their estimated confidence limits. Most of these solutions exhibit R values above 0.75, suggesting that the magnitudes of the σ_2 and σ_3 axes are nearly equal.

Due to the distribution of available FMSs (Fig. 4) the inverted cells are mostly widespread along the Eurasia-Africa plate boundary (Fig. 5). Towards the southwest of Iberia, most of the stress tensors located offshore suggest a NW-SE to NNW-SSE horizontal σ_1, and inclined NE-SW σ_2 and σ_3, with a stress ratio mostly above 0.7, suggesting a prolate stress ellipsoid. In some cells, mainly located in the Gulf of Cadiz, positioning σ_3 close to the vertical. There are some cells also with a high overlap between the σ_2 and σ_3 in their confidence limits, coinciding with high R values, suggesting an almost similar value between both stress axes. In the coastal area and onshore the stress tensors are mostly characterized by NW-SE horizontal σ_1, and NE-SW subvertical σ_2 and subhorizontal σ_3. The cells located in the Lisbon area present more disperse confidence limits. Nevertheless, the data point to stress ellipsoids characterized by NW-SE horizontal σ_1 and both inclined σ_2 and σ_3. The stress ratio decreases from ~0.7 in the south, to 0.5–0.2 near Lisbon, suggesting a prolate shape of the stress ellipsoid in the south, and a triaxial to oblate shape in the north.

The Gibraltar Arc is characterized by a complex stress regime, with varying ellipsoid shapes and orientations depending on the location. In general, the inverted stress ellipsoids present very low dispersion in the confidence limits, suggesting a reliable inversion of the stress field. In the western Betic Cordillera, stress inversion indicated a NW-SE trending subhorizontal σ_1 and subvertical σ_3, with stress ratios above 0.7. The central Betic Cordillera can be divided into two distinct regions. The southern part is characterized by a vertical σ_1, and NE-SW trending σ_3 stress ellipsoids with very low dispersion of the confidence limits. To the north, near the Guadalquivir Basin, the dispersion increases, σ_1 becomes

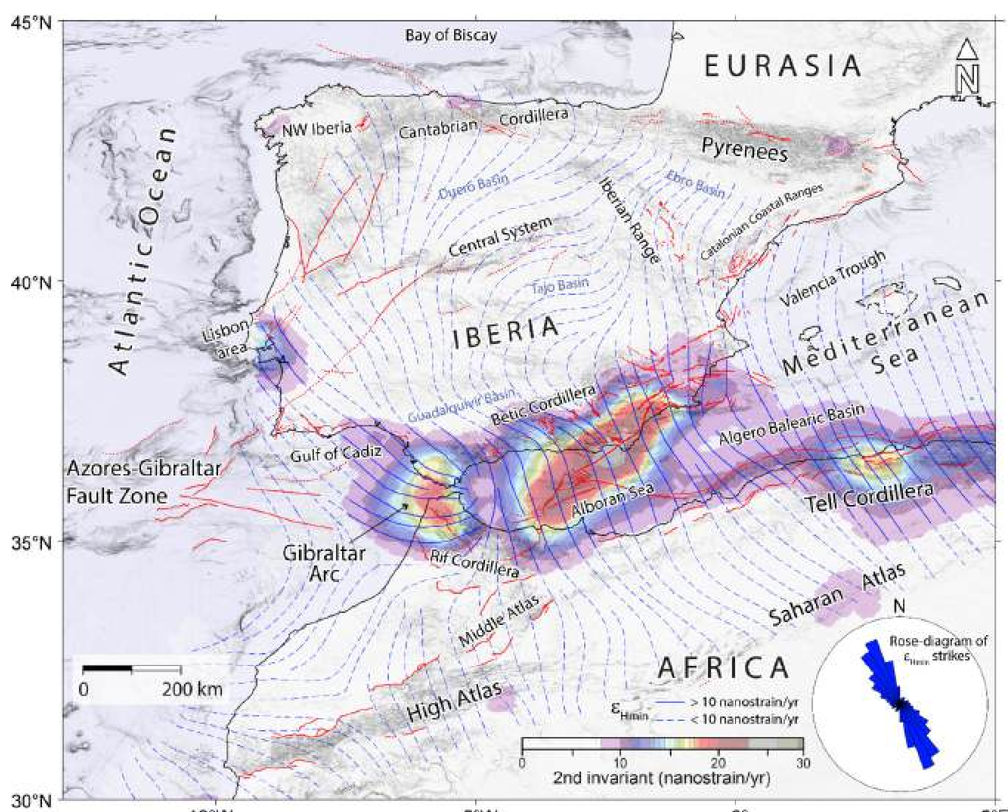

Fig. 9. Second invariant of the strain-rate field. Continuous blue lines represent ε_{Hmin} trajectories in areas where the second invariant exceeds 10 nanostrain/yr and azimuthal uncertainty <30°, while dashed blue lines depict ε_{Hmin} trajectories in other regions where the data have been interpolated. Lower-right inset represents the rose-diagram of the ε_{Hmin} strikes in each grid cell. Active and potentially active faults are marked by solid and dashed red lines, respectively. (For interpretation of the references to color in this figure legend, the reader is referred to the web version of this article.)

horizontal trending NW-SE, while σ_2 locates vertical. In both regions, R values are greater than 0.5, mostly above 0.7, suggesting a triaxial to mainly prolate shape of the stress ellipsoid. In the eastern Betic Cordillera σ_1 is horizontal striking NW-SE to N-S, while σ_3 is horizontal and σ_2 subvertical. In some cells σ_2 and σ_3 rotate, locating σ_2 vertically or both inclined. These cells are mainly located towards the north, a region with higher dispersion in the confidence limits. The stress ratio is irregular in the area, suggesting all prolate, oblate and triaxial shapes. The stress ellipsoids in the eastern Rif Cordillera, the Alboran Sea and on the coast of the central-eastern Betic Cordillera are mainly characterized by NW-SE σ_1 and vertical σ_2, and very different stress ratios. Some ellipsoids with vertical or highly inclined σ_1 and NW-SE striking inclined σ_2 occur surrounding the Alboran Ridge, but with higher dispersion in the confidence limits. Finally, the stress ellipsoids in the western Rif had a close to N-S horizontal σ_1, ENE-WSW inclined σ_2 and σ_3, and prolate shape.

The stress field in the Tell Cordillera is mostly characterized by a horizontal σ_1 striking NW-SE and vertical σ_3, with a prolate shape, as indicated by R > 0.6–0.7. High R values in some cells led to overlapping between the confidence limits of σ_2 and σ_3, as the software struggled to differentiate them due to their proximity in magnitude. In the easternmost and central sector, σ_2 and σ_3 rotate, locating σ_2 vertically or both inclined. Despite greater dispersion in the confidence limits, the three available stress ellipsoids in the High-Middle Atlas suggest a similar pattern. They present horizontal σ_1 striking NW-SE and vertical σ_3. However, R values close to 0.5 suggest a triaxial shape.

The Pyrenees are predominantly characterized by stress ellipsoids with nearly vertical σ_1 and N-S to NE-SW striking σ_3. To the east σ_1 and σ_2 rotate, locating both axes inclined. In the easternmost sector, however, σ_1 becomes subhorizontal, striking NNW-SSE to NNE-SSW, while σ_3 locates subvertical. R values generally ranged between 0.4 and 0.8, suggesting triaxial to prolate ellipsoid shapes. However, in the westernmost Pyrenees R < 0.3 values suggest oblate stress ellipsoids, consistent with the overlapping confidence limits of the σ_2 and σ_1 axes.

In NW Iberia, the inverted four cells illustrated stress ellipsoid with NNW-SSE striking σ_1 and subvertical σ_2, and triaxial to oblate shapes. Stress inversion is possible also in other internal regions of Iberia. The stress ellipsoids in the southeastern Iberian Range and Northeastern Iberian margin showed inclined σ_1 and σ_2 axes striking NW-SE, NE-SW horizontal σ_3, and triaxial to prolate shapes. Finally, to the south of the Central System, stress ellipsoids present a high dispersion in the confidence limits. Regardless, all the stress ellipsoids are characterized by NW-SE striking subhorizontal σ_1 and a subvertical σ_3, and prolate shape.

4.1.2. Maximum horizontal stress field

The horizontal maximum stress (σ_{Hmax}) field showed generally good coverage across the study area (Fig. 5a). Data obtained from stress inversion results (represented by continuous dark red lines) cover the Eurasia-Africa plate boundary, the Pyrenees, the High-Middle Atlas and several regions in northwest and eastern Iberia. The σ_{Hmax} field is further complemented by individual FMSs with M > 4.5 and other stress indicators (Fig. 5a; Table S3); however, these results should be interpreted with caution due to greater uncertainty.

The general pattern of the σ_{Hmax} along Iberia and Northwestern Africa is mostly striking N150°–160°E (inset in Fig. 5). This general pattern slightly rotates counterclockwise in southwestern Iberia and clockwise in the Cantabrian region and eastern Iberia. The Betic-Rif Cordillera has the most complex σ_{Hmax} pattern of the study area. In the western Betic Cordillera the σ_{Hmax} slightly rotates clockwise to ~N130°E while in the western Rif rotates clockwise to ~N20°E. In this way, the σ_{Hmax} pattern locates oblique to the western Gibraltar Arc. The central Betic Cordillera is characterized by a local counterclockwise rotation of the trajectories to ~N120°E. To the easternmost Betic Cordillera the pattern rotates clockwise to ~N5°E. The pattern changes in the Pyrenees and the Iberian Range, where the σ_{Hmax} rotates to ~N100°E, subparallel to the axis of each mountain range.

4.2. GNSS-based velocity field

The horizontal velocity field shown in Fig. 6 provides extensive coverage of the study area. GNSS station density is notably higher in Iberia and the south of France compared to Northwestern Africa. The densest regions are the Pyrenees, the eastern Central System, southwestern Iberia, and the eastern Betic Cordillera, due to the inclusion of various episodic networks in these areas. However, although station density is greater, the current sampling of velocity field is characterized by large uncertainties (up to 0.8 mm/yr) mainly due to the short time series of the measured benchmarks.

In the Eurasia reference frame (Fig. 6a), the most distinct observation is the Eurasia-Africa convergence represented by a northwestward motion in the east and a west-northwestward motion in the west of Africa respect to Eurasia, at rates of 4.5–6 mm/yr. Along the Tell Cordillera the convergence rate decreased to 2–3 mm/yr in the coast. Iberia shows an almost stable pattern with respect to Eurasia, mainly in the northern half. However, velocities increased from 0–0.5 mm/yr in the northeast to 2–3 mm/yr at the southern and southwestern margins. Additionally, the direction of motion rotated from predominantly southwestward in the northeast to west-southwestward in the south-central region and to west-northwestward in the southwest. This general pattern shifts in the western Gibraltar Arc and the eastern Betic Cordillera. The Gibraltar Arc is characterized by westward velocities exceeding 3 mm/yr in the western and central-south Betic Cordillera and reaching 5–6 mm/yr in the Rif Cordillera. Meanwhile, the coastal areas of the eastern Betic Cordillera exhibited a radial motion pattern, with northwestward to northward velocities reaching up to 2 mm/yr.

In the Africa reference frame (Fig. 6b), the Eurasia-Africa convergence is also clearly observed. It is represented by the southeastward motion in northeast Iberia to east-southeastward motion in southwest Iberia. The African reference frame allowed to better observe the motions of different tectonic regions in Northwestern Africa. Most of the stations located in mainland regions showed velocities below 1–1.5 mm/yr. Moreover, it perfectly shows the southwestward motion up to 3.5 mm/yr of the Rif Cordillera. Finally, the Tell Cordillera underwent southeastward decreasing from 2-3 mm/yr on the coast to almost stable in the internal region.

4.3. Geodetic strain-rate field

4.3.1. Horizontal strain-rate field

The strain-rate field is represented by the horizontal maximum and minimum strain axes, the areal change rates (Fig. 7), and the second invariant of the strain (Fig. 9). The highest strain-rate and second invariant values (>10 nanostrain/yr) are located along the Gibraltar Arc and the Alboran Sea, followed by the Tell Cordillera and the Lisbon area (Figs. 7 and 9).

In the Gibraltar Arc and the Alboran Sea, three sectors can be differentiated (Figs. 7 and 9). The data in these regions consistently show low uncertainties—typically below 5 nanostrain/yr for principal strain-rates axes and the second invariant, and under 7 nanostrain/yr for the areal change rate—highlighting their high quality (Fig. S2). First, the westernmost Gibraltar Arc characterized by shortening up to −20 nanostrain/yr in E-W direction and −7 nanostrain/yr in N-S direction. Therefore, this area stands out with the highest negative areal change rates in the region, up to −22 nanostrain/yr. Second, a NE-SW striking corridor from the eastern Rif to the eastern Betic Cordillera, crossing the Alboran Sea (Fig. 7), characterized by NNW-SSE shortening up to −24 nanostrain/yr and WSW-ENE stretching up to 22 nanostrain/yr and the highest second invariant values, up to 30 nanostrain/yr (Fig. 9). The areal change rates in the former region varied between null and slightly negative areas, the latter affecting the central Alboran Sea and the easternmost Betic Cordillera. The data in the eastern Betic Cordillera show the highest uncertainties in the region (Fig. S2), likely due to the high density of stations belonging to different velocity fields. Third, the central Betic Cordillera is characterized by a NE-SW to NNE-SSW stretching up to 17 nanostrain/yr and limited perpendicular shortening. Therefore, it lies under positive areal change rates close to 8–10 nanostrain/yr.

The estimation of the strain-rate field in the Tell Cordillera shows low uncertainties successfully indicating a NW-SE shortening between 12 and 17 nanostrain/yr (Figs. 7 and 9). The central sector exhibits distinct strain patterns, combining maximum shortening (17 nanostrain/yr) with orthogonal NE-SW extension (12 nanostrain/yr). Overall, the Tell Cordillera exhibits negative areal strain-rates, with a maximum contraction of 8–9 nanostrain/yr in both eastern and western sectors. In contrast, the central sector shows significantly lower contraction rates of 0–4 nanostrain/yr. In the Lisbon area, the strain-rate field shows slightly higher uncertainties (~7 nanostrain/yr) but indicates consistent NE-SW extension (up to 17 nanostrain/yr) and probable NE-SW shortening (6–7 nanostrain/yr), yielding slightly positive areal dilatation rates.

The internal regions of Iberia and Northwestern Africa and the Pyrenees underwent low crustal strain-rates, mostly with second invariant values lower than 10 nanostrain/yr (Fig. 9). They depict a disordered pattern of horizontal strain axes and areal changes rates. This pattern stands out in Iberia and the Pyrenees, where higher uncertainties in the estimation of principal strain axes and their derivative products (Fig. S2) make it difficult to accurately determine strain parameters.

4.3.2. Rotational strain-rate field

The rotational strain-rates range between −12 and 14 nanorad/yr (Fig. 8). Consistent with the patterns observed for minimum and maximum strain-rates, and the areal change rates, the maximum rotational deformation occurs along the plate boundary. The western central Betic Cordillera shows the highest values (13–14 nanorad/yr), indicating clockwise rotation. The Tell Cordillera follows this same rotational pattern but with lower rates (5–10 nanorad/yr). Mainland Iberia also exhibits clockwise rotation, though with weaker rates below 4–5 nanorad/yr. Regions with negative values—reflecting counterclockwise rotation—include the eastern Betic Cordillera, where values reach −11 nanorad/yr and estimation errors peak at 9 nanostrain/yr in some grid cells. Other areas with moderate negative rates include the Lisbon area, eastern Pyrenees, and High and Middle Atlas.

4.3.3. Minimum horizontal strain-rate

The minimum horizontal strain-rate axes (ε_{Hmin}) generally align with the shortening direction and is represented by trajectories derived from the combination of ε_{Hmin} strikes estimated in each cell (Fig. 9). These trajectories were calculated only for cells with azimuthal uncertainties below 30° (Fig. S2c). Cells with uncertainties exceeding 30° are widespread across central/northern Iberia and the Pyrenees (Fig. S2c). Nevertheless, we resolved the regional trajectory pattern across most of the study region using cells with lower uncertainties, except for the Pyrenees and NW Iberia.

Areas with uncertainties below 30° (Fig. S2c), located in southern Iberia and Northwestern Africa, are considered representative of the strain-rate field, particularly in the plate boundary and Lisbon area, where the second invariant exceeds 10 nanostrain/yr. On the opposite, high uncertainties in ε_{Hmin} strikes, coupled with second invariant values below 10 nanostrain/yr, in central/northern Iberia and the Pyrenees, indicate the absence of a clear strain pattern, thus, results should be interpreted cautiously.

As represented in the rose-diagram, most of the estimated ε_{Hmin} strikes indicate that the region is affected by N150°-160°E shortening (inset in Fig. 9). This general shortening affects the High and Middle Atlas, Tell Cordillera, the easternmost Rif and the Alboran Sea, as well as southwestern Iberia. This general pattern rotates counterclockwise in the central Betic Cordillera, up to N110°E, and clockwise in the eastern Betic Cordillera, up to N010°E. The main strike-change of the trajectories occurs in the western Gibraltar Arc. This region is characterized by a radial pattern of the trajectories respect to the curved axis of the arc; striking NE-SW in the western Betic Cordillera, E-W in the Strait of Gibraltar, and WSW-ENE in the western Rif Cordillera.

5. Discussion

The newly computed stress and strain-rate fields provide fresh insights into the active tectonic and geodynamic processes shaping Iberia and Northwestern Africa. Our discussion addresses two principal aspects:

a) Consistency between deformation indicators. By comparing stress fields, strain-rate distributions, and fault kinematics, we evaluate their mutual consistency and associated uncertainties. This integrated analysis refines our understanding of tectonic activity across major regional structures.
b) Geodynamic implications. We explore how these datasets elucidate the processes influencing each region, particularly their spatial relationships and roles within the Eurasia-Africa plate boundary.

5.1. Stress and strain-rate fields and active structures

The stress inversion based on the definition of seismotectonic zones (e.g., Zoback and Zoback, 1980; Rigo et al., 2015; Villani et al., 2024) implies a deep geological and seismological understanding of the region, which is not free from interpretative errors and biases. Additionally, Neogene geological information sometimes differs from explicitly active processes (e.g., Berberian, 1995; Costa et al., 2000; Ruiz-Constán et al., 2009; Madarieta-Txurruka et al., 2024). To avoid the mentioned uncertainties, for the first time, a stress inversion within a 0.5°×0.5° grid-based approach has been computed, covering Iberia and Northwestern Africa and using a large dataset of FMSs (Table S2). Moreover, this approach facilitates comparison with the new grid-based strain-rate field (Figs. 7 and 8; Shen et al., 2015). In the following section, we compare the obtained stress field and strain-rate field with previous results.

In addition, the results are analyzed in relation to the mapped active faults. According to Anderson (1905), the orientation of principal stress axes constrains the expected faulting regimes in a region (Fig. 5). At the crust surface normal faulting occurs when σ_1 is vertical, strike-slip faulting occurs when σ_2 is vertical, and thrusting occurs when σ_3 is vertical (Anderson, 1905). The recognition of tectonically active structures is also linked to the active surface deformation that the GNSS velocity field has successfully identified. The second invariant of the strain field (Fig. 9) reflects the zones with maximum deformation and serves to compare with the location and/or concentration of active faults in each area (Fig. 2). On the other hand, the areal change (Fig. 7) provided a valuable metric for comparison of contraction/dilatation within the crust with kinematics of faults.

Overall, the stress field (inset Fig. 5) shows a regional N150-160°E oriented compression which aligns with the NW-SE Eurasia and Africa convergence shown by the velocity field presented here (Fig. 6). Both results agree with previous estimations (e.g., Herraiz et al., 2000; de Vicente et al., 2008; Fadil et al., 2006; Koulali et al., 2011; Palano et al., 2013b, 2015). The strain-field (Figs. 7 and 8) improves the previous estimation focusing on the entire Iberia and NW Africa (Garate et al., 2015), and suggests that the convergence results in an overall N150-160°E shortening (inset in Fig. 7) accumulated along the plate boundary (Fig. 9), where most of the previous strain-rate fields are computed (e.g., Palano et al., 2013b; Sparacino et al., 2020; Billi et al., 2023). However, this general stress–strain field is altered due to the high complexity of the plate boundary, as described below.

5.1.1. Active faulting along the Eurasia-Africa plate boundary

The Azores-Gibraltar Fault Zone offshore SW Iberia presents significant challenges for direct geodetic strain estimation, yet the intense historical and instrumental seismicity clearly demonstrates active tectonic deformation. The new stress field revealed a consistent NNW-SSE orientation of σ_1 along this complex plate boundary, generally agreeing with previous results – whether uniaxial compression (de Vicente et al., 2008) or a *trans*-pressive regime (Stich et al., 2006). These apparent discrepancies likely reflect genuine spatial variations in the stress field, as evidenced by our identification of different stress regimes (vertical σ_2, vertical σ_3, or inclined σ_2-σ_3). Three distinct domains are characterized remarkably by aligning with seismotectonic zonation proposed by Palano et al. (2013b). The Southwestern Iberian margin shows predominantly vertical σ_2 configurations, the Gulf of Cadiz domain displays vertical σ_3 orientations, while the western Azores-Gibraltar Fault Zone shows both inclined σ_2 and σ_3 (Fig. 5). The pattern in the Gulf of Cadiz correlates well with the known distribution of ENE-WSW reverse faults and WNW-ESE dextral strike-slip systems (Martínez-Loriente et al., 2013, 2014, 2018; Gràcia et al., 2003; Zitellini et al., 2004). Notably, our data perfectly reflects the sinistral component along NW-SE trending thrust faults in the western Azores-Gibraltar Fault Zone not previously emphasized in Quaternary fault catalogs (Fig. 2), but consistent with FMS (Buforn et al., 1988; Pro et al., 2013) (Fig. 4).

Our analysis revealed remarkably complex stress and strain-rate fields across the Gibraltar Arc, refining previous models that proposed a broadly uniform *trans*-tensive to strike-slip regime (de Vicente et al., 2008). This complexity not only matches the distribution of known active faults (Fig. 2), validating our inversion approach, but also provides new insights into regional deformation patterns. The corridor tracing through the Alboran Sea into the eastern Betic Cordillera formed by stress ellipsoids with vertical σ_2 agrees with previous estimations (Stich et al., 2006; Palano et al., 2013b) and precisely follows the seismically active Trans-Alboran and Eastern Betic shear zones – corridor dominated by strike-slip faulting that have been extensively documented (Silva et al., 1993; Galindo-Zaldívar et al., 2018). This corridor coincides with the region with higher second invariant values, reaching rates up to 30 nanostrain/yr, and shortening values up to 8 nanostrain/yr, also evidenced by Sparacino et al. (2020) (Figs. 7 and 9), consistent not only with sinistral fault motions (Stich et al., 2006; Echeverría et al., 2015) but also with the activity of NE-SW folds like the Alboran Ridge and Águilas Arc (Coppier et al., 1989; Gómez de la Peña et al., 2022; Ercilla et al., 2022). In contrast, our results reveal a significant nuance in the Eastern Betic Shear Zone, where the stress field exhibits a more compressional character than indicated by previous regional inversions (Stich et al., 2006; Palano et al., 2013b), particularly along its northern front. The strain-field similarly reflects N-S shortening along the eastern Betic Cordillera (Fig. 7). However, the highest values are located southward close to the Aguilas Arc, where transpressive to strike-slip stress regime indicate persistent N-S compression (Fig. 5). While these strain-rates coincide with areas of highest uncertainty, the observed ε_{Hmin} rates (~30 nanostrain/yr) align with both local geodetic measurements suggesting 30–50 nanostrain/yr N-S shortening across the Aguilas Arc (Echeverría et al., 2013; Portela et al., 2025), and kinematic evidence from active WSW-ENE thrust systems (Fig. 2) (García-Mayordomo and Martín-Banda, 2022).

In the western Betic Cordillera, the limited but consistent FMSs depict a NW-SE oriented σ_1 perpendicular to the arc, aligned with previous results (Ruiz-Constán et al., 2009, 2011; Palano et al., 2013b). The eastern Rif presents a markedly different stress configuration, characterized by N-S horizontal σ_1 and subvertical σ_3 that appears oblique to the arc shape (Fig. 2). Most strikingly, the new velocity field and strain-rate field support the westward displacement (e.g., Koulali et al., 2011; González-Castillo et al., 2015a) revealing the highest shortening rates (up to −20 nanostrain/yr) along the western Gibraltar Arc, findings that correlates with active thrusting in the Rif Cordillera (Fig. 2). On the opposite, absence of identified active faults in the western Betic Cordillera contrasts with the stress–strain field, suggesting either: a) deformation is being accommodated through blind thrust systems (e.g., Pedrera et al., 2011; González-Castillo et al., 2015a,b), or b) current fault mapping in the western Betic Cordillera requires revision. An interesting feature is the clear angular discrepancy of up to 90° between the estimated ε_{Hmin} and σ_{Hmax}. Assuming macroscopically homogeneous and elastic crustal blocks, the strain field should align with the stress field, and therefore, the regional fields should be parallel. However, while the σ_{Hmax} is oriented NW-SE to N-S, the ε_{Hmin} shows a radial pattern relative to the arc. The low seismicity in the western Gibraltar Arc, resulting in limited availability of FMSs, explains this discrepancy, aseismic stress relaxation goes unrecorded. Thus, the σ_{Hmax} keeps reflecting mainly the NW-SE Eurasia-Africa compression, while the ε_{Hmin} indicates the westward aseismic displacement of the western Gibraltar Arc.

The stress field pattern in the central Betic Cordillera reveals a consistent tectonic signature characterized by NE-SW oriented to radial extension. This configuration, which aligns with numerous previous stress inversions (Galindo-Zaldívar et al., 1999; Herraiz et al., 2000; Stich et al., 2006; Madarieta-Txurruka et al., 2021, 2022, 2024), together with ENE-WSW to NE-SW dilatation-rates up to 10 nanostrain/yr (Fig. 7), reflects the region dominant extensional regime. The ENE-WSW to NE-SW stretching of the central Betic Cordillera, well-documented in recent works (Galindo-Zaldívar et al., 2015; Sparacino et al., 2020; Martín-Rojas et al., 2023), is consequence of the activity of well-studied NW-SE striking normal faults (Sanz de Galdeano et al., 2012). A stress transition occurs northward toward the Guadalquivir Basin, where vertical σ_2 orientations correlate with N-S trending strike-slip fault systems in a low strain-rate area (Pedrera et al., 2013; Tendero-Salmerón et al., 2020).

The Tell Cordillera displays a tectonic regime marked by persistent deformation, as evidenced by strain-rates consistently exceeding 10 nanostrain/yr. These elevated values correspond spatially with both increased fault density and heightened historical and instrumental seismicity (Figs. 2 and 3). The well-constrained dominant NW-SE shortening and the obtained stress pattern (characterized by NW-SE oriented σ_1 and predominantly vertical σ_3), confirm previous seismic (Stich et al., 2006; de Vicente et al., 2008; Palano et al., 2013b) and geodetic estimations (e.g., Sparacino et al., 2020; Billi et al., 2023). This stress–strain configuration explains the prevalence of ENE-WSW to NE-SW thrust faults (Meghraoui, 1991; Bouhadad, 2001) (Fig. 2). The detailed stress analysis reveals additional complexity through the identification of stress domains with vertical σ_2 and inclined σ_2-σ_3. These variations correlate closely with segments where WNW-ESE dextral strike-slip systems disrupt the continuity of the thrust system (Mauffret, 2007).

5.1.2. *Active faulting along intraplate regions*

Second invariant strain-rates in Iberia, the Pyrenees, and the Moroccan Atlas are significantly lower compared to regions along the plate boundary (Fig. 9). The low values contrast with the location of recognized faults (Fig. 2) and the historical and instrumental seismicity (Figs. 3 and 4) in some of these areas. This data suggest that they correspond to structures with very low Quaternary activity, undetectable within the measurement period, and/or that they would respond to processes governed by vertical deformation.

Our improved FMS catalog provided new insights into the stress field patterns across western Iberia. In the Lisbon area, the data reveal a clear NW-SE oriented σ_1 and transpressive to strike-slip stress regime, as evidenced by the higher dispersion of the confidence limits and the partial overlapping between σ_2 and σ_3. The stress field is consistent with NNE-SSW trending reverse to strike-slip faults (Cabral, 2012; Carvalho et al., 2011; Baptista et al., 2014). The consistently high second invariant values indicate significant surface deformation (Fig. 9). The computed strain-rate field reveals strike-slip to transtensive kinematics in the region, showing slight divergence from the pure strike-slip regime proposed by local studies (Fonseca et al., 2021) and with the stress field, confirming however the significant tectonic activity of the area (e.g., Stich et al., 2005). Nevertheless, the apparent discrepancy between the transpressive stress field and the strike-slip to transtensive strain-rate field may reflect the influence of thick Cenozoic sedimentary cover in Lisbon area (Carvalho et al., 2017). This suggests that shallow deformation adjustments within the sedimentary sequence could be the surface expression linked to the displacement of deep-blind thrusts (Cabral et al., 2013). Moving northward, the stress pattern shift to a stress regime mainly characterized by vertical σ_2 and NNW-SSE oriented σ_1, aligning with earlier inversion results (Herraiz et al., 2000; Stich et al., 2006; de Vicente et al., 2008), but also stress ellipsoids defined by NNW-SSE inclined σ_1 and σ_2. This stress configuration and low strain-rate values (Figs. 7 and 8) appears coherent with the predominantly low slip-rate strike-slip faulting (Villamor et al., 2012; Cabral, 2012; López-Fernández et al., 2018; Fernández-Viejo et al., 2021) (Fig. 2). The inclined σ_1 and σ_2 appears to be influenced by the few available FMSs of low-magnitude earthquakes, which could be related to local stress perturbations rather than the regional pattern (Martín-González et al., 2023).

The Pyrenean stress field confirmed the predominant vertical σ_1 orientation also documented in other regional-scale studies (Herraiz et al., 2000; de Vicente et al., 2008; Rigo et al., 2015), while providing new details about horizontal stress orientations. The observed N-S to NE-SW oriented σ_3 generally aligns with de Vicente et al. (2008) and Rigo et al. (2015) results, though contrasts with the E-W striking σ_3 reported by Herraiz et al. (2000). This discrepancy is likely explained by the high R-ratio values ($R > 0.75$) across the Pyrenees (Fig. 5b) and the chaotic strain-rate pattern (Fig. 7). Importantly, the computed stress field is consistent with the presence of active E-W normal faults (Lacan and Ortuño Candela, 2012) and local GNSS studies, suggesting N-S stretching (Asensio et al., 2012). The stress transition to compressional/*trans*-tensional stress regime observed in some cells in the easternmost Pyrenees agrees with Rigo et al. (2015) results. But in contrast, they obtained a strike-slip stress regime along the entire eastern Pyrenees. This can be attributed to their limited FMSs distribution (concentrated eastward). Our expanded catalog instead, reveals a more extensional regime also in the central-eastern sector, consistent with mapped E-W and ENE-WSW normal fault systems (Lacan and Ortuño Candela, 2012) (Fig. 2). Although the Pyrenees exhibit recurrent seismicity, the generally low magnitudes align with low strain-rates across the mountain range. Unfortunately, these low strain-rate values—combined with high uncertainties—preclude robust tectonic interpretations from the new strain-rate field (Figs. 7–9).

Further south, in the Iberian Range, stress field with close to vertical σ_1 orientations and R-values exceeding 0.5, combined with low strain-rates, suggest a low-rate extension through normal faults orthogonal to the regional compression (Gutiérrez, 2012). As observed in the Iberian Range, it is important to note that the main sedimentary basins of Iberia (Duero, Ebro, and Tajo) exhibit significant discrepancies in ε_{Hmin} and σ_{Hmax} orientations, with differences reaching up to 90° (Figs. 5 and 7). However, as previously noted, these regions are characterized by very low strain-rates (Fig. 9), where uncertainties—particularly in the azimuthal orientation of the principal strain-rate axes—are exceptionally high (Fig. S2). Consequently, ε_{Hmin} likely does not represent well-constrained tectonic shortening. Moreover, these areas generally display low tectonic activity (García-Mayordomo and Martín-Banda, 2022) and no seismicity, except for the Tajo Basin. The stress field, which was difficult to estimate directly in the Tajo Basin (see confidence limits in Fig. 5) and had to be extrapolated in the other basins from surrounding regions, aligns more consistently with the regional pattern. So, we therefore suggest that σ_{Hmax} more reliably reflects the geodynamic imprint, while ε_{Hmin} exhibits unexpected patterns, likely due to high uncertainties or local effects.

Finally, the NW-SE compressional stress regime observed in the High Atlas aligns with previous stress inversion studies (Levandowski, 2023; Skikra et al., 2025) and is consistent with the dominant reverse faulting mechanisms (Arboleya et al., 2004). Moreover, the southern stress ellipsoids exhibit significant overlap between the σ_2 and σ_3 axes, reflecting inherent challenges in stress field estimation within this cell. This observation likely relates to the presence of strike-slip FMSs, which aligns with field evidence of active transcurrent faulting in the region (Gomez et al., 1996). The consistent NNW-SSE oriented shortening, though with low-rates (Fig. 7 and S2), agrees with the σ_1 and σ_{Hmax} strikes (Fig. 9) and may further contribute to tectonic activity in the region.

As shown here, the stress field is in general accordance with the structural data being coherent with the strain-rate field. The novel grid-based methodology increased the knowledge of the study area, mostly in accordance with the different zonation proposed in the literature (e.g., Herraiz et al., 2000; Stich et al., 2006; de Vicente et al., 2008; Palano et al., 2013b). Therefore, this methodology could become a valuable tool for determining or redefining seismotectonic zones. However, it also implies some limitations. First, it is a method dependent on FMS availability, which is correlated with the densest seismic areas (Fig. 5). Thus, some areas could present a lack of inverted cells due to the low number of available FMSs, as occurred in the Atlas and NW Iberia. Second, the inversion is not reliable in cells bordering/over two different seismotectonic zones because the method considers FMSs derived from different stress regimes (Fig. 5). On the other hand, this limitation could help in detecting unknown seismotectonic boundaries. Additionally, the scale of observation depends on the resolution of the grid and the cell size. For local studies higher resolution is required and thus, the number and spatial coverage of available FMSs must increase. Therefore, while this approach is valuable for regional-scale research, such as the westernmost Mediterranean, its relevance in local studies needs further evaluation.

5.2. Geodynamic implications

The comparison between stress and strain-rate fields reveals crustal deformation patterns driven by regional stresses, offering a framework to discuss underlying geodynamic mechanisms. In the following sections we offer new insight in the new and old processes shaping the Eurasia-Africa plate boundary, the role of the Gibraltar Arc and how stresses are transferred to the internal parts of the main plates.

5.2.1. The complex Eurasia-Africa plate boundary in the Atlantic-Mediterranean transition

As shown before the convergence between Eurasia and Africa plates results in compression and shortening along the plate boundary in the South Iberian and Northwestern African margins, implying a complex interaction between the involved crustal blocks. A good example of the complexity is the ongoing debate to define the Eurasia-Africa plate boundary in the region (e.g., Bird, 2003; Gutscher, 2004; Gómez de la Peña et al., 2022; Billi et al., 2023).

As described below the plate boundary is determined by the development of the Gibraltar Arc. Our results led to divide the plate boundary in four sectors —Atlantic, Gibraltar, Alboran and Algero-Balearic— based on the stress pattern, the localization of deformations, and the number and nature of the involved crustal domains (Fig. 10 and Table 1). From east to west, the sectors can be divided as follows:

a) The *Atlantic sector* is the result of the direct interaction between the Atlantic oceanic crust, the Southwestern Iberian margin (Eurasia) and the old and cold Jurassic oceanic lithosphere of the Gulf of Cadiz (Martínez-Loriente et al., 2013) (Fig. 10). Hypocenters and FMSs suggest that the deformation localize to the north of the Gulf of Cadiz Oceanic Crust (GCOC) in NE-SW/NNE-SSW reverse to sinistral and WNW-ESE dextral faults (Buforn et al., 1988; Pro et al., 2013) cutting the entire oceanic lithosphere (Figs. 3 and 4). This deformation pattern develops under NW-SE compressive stresses, characterized by alternating vertical σ_2 and σ_3 principal stress orientations throughout the sector. Therefore, this sector constitutes a *trans*-

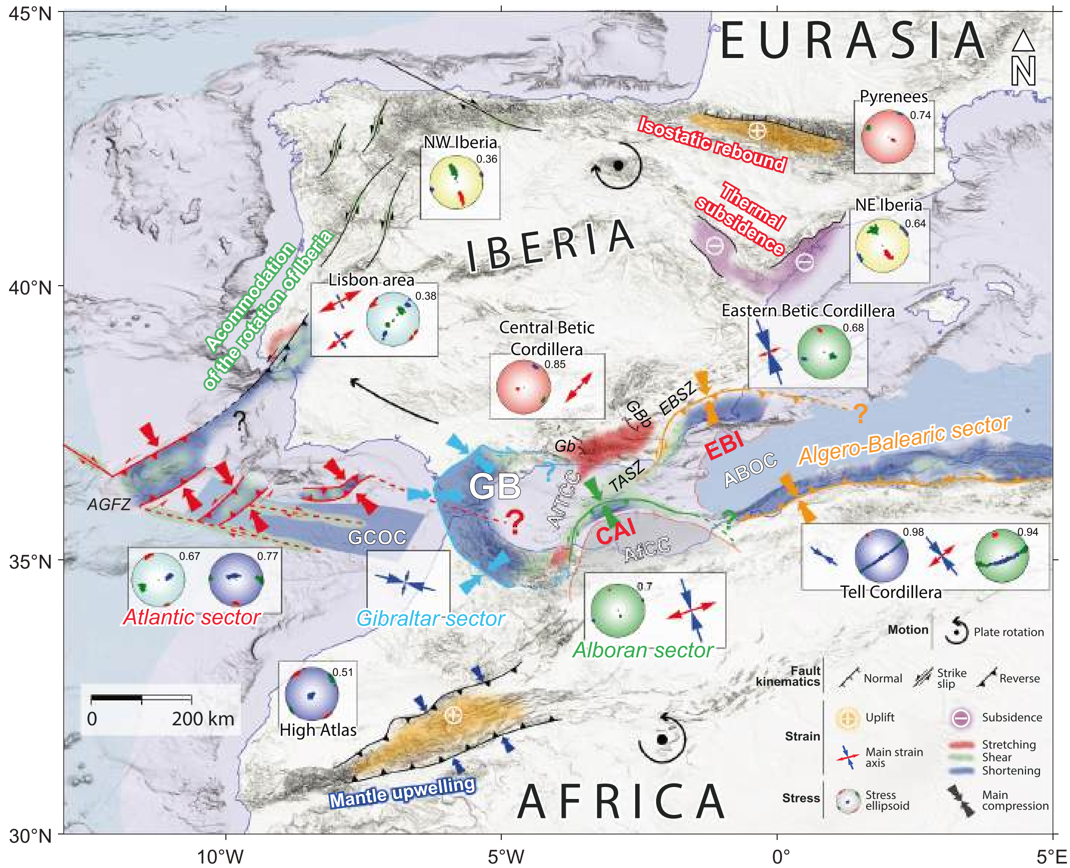

Fig. 10. Geodynamic model of Iberia and Northwestern Africa. The four sectors along the Eurasia-Africa plate boundary are depicted. Boxes represent the most representative stress and strain axes in each region. The number adjacent to the stereoplots indicates the stress ratio (R). WGA: Western Gibraltar Arc. ABOC: Algero-Balearic Oceanic Crust. AlTCC: Alboran thinned continental crust. AfCC; African continental Crust. CAI: Central Alboran indentation. EBI: Eastern Alboran indentation. AGFZ: Azores-Gibraltar Fracture Zone. EBSZ: Eastern Betic Shear Zone. TASZ: Tran-Alboran Shear Zone. Gb: Granada Basin. GBb: Guadix-Baza Basin.

pressive boundary formed by en-echelon thrusts and large WNW-ESE dextral faults (Zitellini et al., 2009; Martínez-Loriente et al., 2013, 2018). To the west, the Atlantic Eurasian and African oceanic crust overthrust each other. To the east, GCOC and the thinned Southwestern Iberian margin overthrust each other (Galindo-Zaldívar et al., 2003; Sallarès et al., 2011; Martínez-Loriente et al., 2014).

b) The *Gibraltar sector* involves the western Gibraltar Arc, formed by the western Betic Cordillera and the Rif Cordillera, located between the two main plates. As shown by the velocity field, the western Gibraltar Arc displaces independently westward and overthrust the Iberian and African margins (Fig. 5). The strain-rate field shows an internal shortening and suggests that the plate boundary is divided into two branches. The southern branch has well-defined two zones: the western zone is characterized by large E-W shortening and negative areal change rates coinciding with the Rif Cordillera external front. Therefore, the plate boundary agrees with the proposal of Billi et al. (2023). Towards the east the boundary is more diffuse. The low areal strain-rates indicate comparable magnitudes of N-S shortening and E-W extension along this region. Moreover, here is suggested a northern branch, defined by the western Betic front (González-Castillo et al., 2015b) and a NE-SW dextral corridor (Ruiz-Constán et al., 2009; Fadil et al., 2006). The highest rotational strain-rates in the study area are concentrated in this region, indicating a kinematic transition between the central and western Betic Cordillera (Fig. 8). The independent behavior of the western Gibraltar Arc can be explained by the active subduction with rollback (Pedrera et al., 2011; González-Castillo et al., 2015a; Duarte et al., 2024). The highest shortening rates presented here (Fig. 7) supports at least the decrease of the subduction and influence of mantle flow due to slab sinking (Neres et al., 2016; Civiero et al., 2020), also supported by numerical modelling (e.g., Gea et al., 2023).

c) The *Alboran sector* is characterized by an Alboran thinned continental crust (AlTCC) between the Betic Cordillera and Africa. The second invariant of the strain-rate field (Fig. 8) suggest that most of the convergence along this sector is accommodated in the Alboran Sea and the northern coastal areas, in accordance with the velocity field published by Galindo-Zaldívar et al. (2022) and geomorphology data (Ercilla et al., 2025). The stress regime and areal change rates indicate that the region is currently deformed by strike-slip faulting coupled with minor shortening component, as evidenced by negative areal-change values, along the active Trans-Alboran Shear Zone (TASZ). This data point to active indentation tectonics due to the northwestward displacement of the central Alboran indenter (Galindo-Zaldívar et al., 2018; Estrada et al., 2018), composed of African Continental Crust (AfCC), into the pre-thinned weak continental crust. This sector is consistent with the boundaries suggested by Gómez de la Peña et al. (2022) and Billi et al. (2023).

d) The *Algero-Balearic sector* involves the young Algero-Balearic oceanic crust (ABOC) located between the Southeastern Iberian and Northwestern African margins. The horizontal strain-rates (Fig. 7) show a N-S to NW-SE shortening localized in the eastern Betic Cordillera and in the Tell Cordillera accommodating the NW-SE compression, in accordance with the previous and the local GNSS networks (Borque et al., 2019; Bougrine et al., 2019; Echeverría et al., 2013, 2015; Portela et al., 2025). The seismicity localization also suggests that most of the deformation in this sector is concentrated in the margins (Figs. 3 and 4). In contrast, the low seismicity and the absence of active faulting agree with the lower strain-rate along the Algero-

Table 1
Geodynamics of Iberia and Northwestern Africa. Comparison between seismicity, stress, strain and the proposed tectonic/geodynamic models for each region. Letters in the seismicity column indicate earthquake kinematics: N (Normal), R (Reverse), SS (Strike-slip). The stress and strain columns depict the most representative stress and strain axes in each region. The number adjacent to the stereoplots indicates the stress ratio (R).

Region			Seismicity	Seismic stress	Geodetic strain-rate		Tectonic/geodynamic
					Strain-rate	2nd invariant	
Eurasia-Africa plate boundary	Atlantic sector		Frequent < 50 km depth moderate to high magnitude seismicity R and SS FMSs	 0.93  0.77	– – – –		Oblique *trans*-pression between Eurasia Oceanic Crust/SW Iberian margin and African Oceanic Crust/Gulf of Cadiz Oceanic Crust (GCOC)/Eurasia-Africa convergence
	Gibraltar sector		Mostly aseismic Crustal low to moderate magnitude seismicity in the edges. Intermediate seismicity N, R and SS FMSs	– – – –		10–20 nanostrain/yr	Westward displacements of the western Gibraltar Arc/Subduction with rollback or mantle flow
	Alboran sector		Frequent crustal low to moderate magnitude seismicity R and SS FMSs	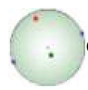 0.62	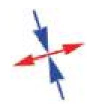	15–30 nanostrain/yr	African Continental Crust (AfCC) indents the Alboran Thinned Continental Crust (AlTCC)/Eurasia-Africa convergence
	Algero-Balearic sector	Eastern Betic Cordillera	Crustal low magnitude seismicity SS and R FMSs	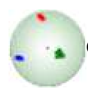 0.65		10–30 nanostrain/yr	Algero-Balearic Oceanic Crust (ABOC) indents the SE Iberian margin/Eurasia-Africa convergence
		Tell Cordillera	Frequent crustal moderate to high magnitude seismicity R and SS FMSs	 0.95		10–20 nanostrain/yr	Underthrusting of the Algero-Balearic Oceanic Crust (ABOC) below Tell Cordillera/Eurasia-Africa convergence
Margin regions	Central Betic Cordillera		Frequent crustal low to moderate magnitude seismicity Mainly N FMSs	 0.8		10–18 nanostrain/yr	Orogen parallel extension/Gravitational stress
	Lisbon area		Scarce crustal low to moderate magnitude seismicity SS and R FMSs	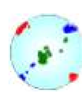 0.5		10–15 nanostrain/yr	Trans-pression and stretching at the surface/Clockwise rotation of SW Iberia + Eurasia-Africa convergence
Intraplate regions	NW Iberia		Scarce crustal low to moderate seismicity SS and R FMSs	 0.36	– – – –	< 10 nanostrain/yr	Large scale slow-rate strike-slip faulting/Clockwise rotation of SW Iberia + Eurasia-Africa convergence
	Pyrenees		Frequent crustal low to moderate magnitude seismicity N and SS FMSs	 0.77			Orogen perpendicular extension/Isostatic rebound in the eroding highlands
	NE Iberia		Scarce crustal low magnitude seismicity SS and N FMSs	 0.64			Orogen perpendicular extension/Post-rift thermal subsidence + regional compression
	High Atlas		Scarce crustal moderate to high magnitude seismicity R and SS FMSs	 0.51			Thrusting and uplift/Mantle upwelling + Eurasia-Africa convergence

Balearic basin. These observations suggest that the rigid Algero-Balearic oceanic crust underwent rotation but low internal deformation (Palano et al., 2015) and underthrusts the Northwestern African margin while indents the Southeastern Iberian margin, delineating a plate boundary previously proposed by Billi et al. (2023).

5.2.2. *The rotation of SW Iberia*

The new velocity field depicts a clockwise rotation of Iberia between 2 and 4 nanorad/yr (Fig. 8), mainly observed in western Iberia and with the highest velocities values in southwestern Iberia (Fig. 6). These values correspond to 0.1–0.2 deg/Ma, slightly higher than the 0.07 deg/Ma estimated by Palano et al. (2015). The higher values in some areas could be related to located features, however, the general rotational pattern agrees with the previous results.

This low rate rotation, mainly affecting western and southwestern Iberia could result from a) the angular relation between the Eurasia-Africa convergence and the orientation of the Iberian margins in each sector, and/or b) the structural differences between the distinct sector of the Eurasia-African boundary, as outlined in the previous section.

The velocity field presented here reflects a convergence shifting from a WNW-ESE direction in the Atlantic to a NW-SE direction in the Mediterranean areas (Fig. 5), probably related to the counterclockwise rotation of Africa relative to Eurasia (e.g., Calais et al., 2003; McClusky et al., 2003; Serpelloni et al., 2007; Neres et al., 2016). This pattern also implies that the convergence in the Mediterranean is nearly perpendicular to the Southeastern Iberian margin, whereas in the Atlantic, it is oblique to the Southwestern Iberian margin. This contrast in convergence angles likely contributes to the observed rotational deformation in southwestern Iberia.

This phenomenon could be further influenced by the presence of the Gibraltar Arc, located between the major plates, as described in the 5.2 section. The new results of the second invariant show that the Alboran Domain and the detached Iberian and African margins absorb most of the convergence (Fig. 9) along the three Mediterranean sectors. In the Atlantic sector, in contrast, there are no microplates between Iberia and Africa, resulting in direct interaction between the two plates. Moreover, seismicity suggests that most of the deformation is accommodated to the south of the Southwestern Iberian margin until 50 km depth (Fig. 3), probably involving the entire oceanic lithosphere (Stich et al., 2007). Therefore, the African push at the lithospheric scale may imply not only the deformation of the margin but also the rotation of SW Iberia. Additionally, the continuous westward displacement of the Western Gibraltar Arc, pushing against SW Iberia, could further enhance its clockwise rotation.

As stated by Palano et al. (2015), the clockwise rotation of SW Iberia implies active thrusting and NNE-SSW sinistral or NW-SE dextral faulting as mechanisms to accommodate stress in NW Iberia. The velocity field presented here suggests that rotation ends in the Lisbon area, while the NW Iberia remains practically stable (Fig. 6). Historical and instrumental seismicity data, FMS with reverse kinematics, and the presence of reverse to sinistral faults in the Lisbon area (Fonseca et al., 2021) indicate that a significant portion of the deformation is concentrated there (Fig. 10 and Table 1). The negative rotational strain-rate values reported in the northwest of the Lisbon area further support this region as a key structural boundary (Fig. 8). Moreover, this is further supported by the highest values of the second invariant (Fig. 9). August 2024, Mw 5.3, earthquake, located in the Western Iberian margin (Fig. 4), with a FMS showing reverse to sinistral motion, suggests that this front may continue offshore. Indeed, the southern part of the Western Iberian margin is characterized by Alpine compressional structures (Alves, 2024).

As shown, the data suggest that a significant portion of the stress is accommodated in the Lisbon area. However, part of it could be transferred toward NW Iberia (Fig. 10 and Table 1) activating low-rate sinistral and dextral faults in NW Iberia (López-Fernández et al., 2018; Fernández-Viejo et al., 2021; Martín-González et al., 2023). The frequent low to moderate magnitude seismicity in the region (Fig. 2) suggests this behavior, in response to a NW-SE compression (Fig. 5).

5.2.3. *The extension in the central Betic Cordillera*

As described before, the stress field suggest radial to NE-SW oriented extension along the central Betic Cordillera while the strain-rate field shows significant dilatation-rates mainly in NE-SW direction. These data support the previous observations (e.g., Stich et al., 2006; Madarieta-Txurruka et al., 2021, 2022; Martín-Rojas et al., 2023). As shown in the velocity-field, the central Betic Cordillera lies between the westward displacing, western Betic Cordillera and northwest-northward displacing eastern Betic Cordillera, and therefore the extension in the central Betic Cordillera could result from the opening between the western and eastern Betic Cordillera (Fig. 10 and Table 1), implying the subsidence of the region. However, the region underwent the highest uplift since the middle Miocene (Braga et al., 2003; Reinhardt et al, 2007) and constitutes the highest elevation in entire Iberia (Sanz de Galdeano and Alfaro, 2004), pointing to an extension running parallel to the arc and orthogonal to the regional compressive stress. However, as previously noted, the nearly radial extension pattern rules out NW-SE compression. Furthermore, the ε_{Hmin} axes exhibit near-zero values —significantly lower than those in the nearby Alboran Sea (Galindo-Zaldívar et al., 2022)— confirming the absence of shortening in this area. Additionally, the active normal faulting mainly occurs surrounding the elevated areas (Sanz de Galdeano et al., 2012; Martínez-Martos et al., 2017; Martín-Rojas et al., 2023). The combination of the observations suggest that gravitational forces are the main features controlling the extension, and not the compression (Palano et al., 2013b; Madarieta-Txurruka et al, 2023, 2024).

Some authors, such as Gutscher (2004) or Koulali et al. (2011) suggest a dextral plate boundary along the northern limit of the central Betic Cordillera. Low second invariant values compared to the Alboran Sea point to a gradual decrease of the deformation toward the north of the central Betic Cordillera (Figs. 7 and 8). In contrast, the stress-field and FMSs could imply the activity of E-W dextral faults (Fig. 3), however, detailed studies point to an activity of a small N-S sinistral faults (Carmona et al., 2009; Pedrera et al., 2013; Tendero-Salmerón et al., 2020). Thus, new data support that the central Betic Cordillera is currently almost attached to the Southern Iberian margin, and the plate boundary is shifted toward the south, where the thinned Alboran crust accumulates the deformation.

5.2.4. *Low deforming intraplate active regions*

In contrast to the Eurasia-Africa plate boundary, the intraplate tectonically active regions exhibit low strain-rates (Fig. 9). As discussed before, the low-to-moderate magnitude seismicity related to sinistral and dextral faults in NW Iberia agrees with the general NW-SE compressional regime of Iberia. However, the stress–strain patterns along the Pyrenees, NE Iberia, and the High Atlas needs further discussion.

Low strain-rates across the Pyrenees (Figs. 7 and 8) and the chaotic pattern of dilatation-rates at the scale of the entire range contrast with the recurrent seismicity, which primarily occurs in the western part of the Pyrenees (Fig. 2). Main earthquakes in the area, consequence of the activation of normal faults under the N-S extensional stress calculated here (Fig. 5), support the model proposed by Lacan and Ortuño Candela (2012). They suggest an uplift of the mountain range due to an isostatic adjustment in response to erosion. As pointed out by them, the normal faults and the seismicity occurs to the north of the highest massifs of the cordillera, which undergo continuous uplift (e.g., Ortuño et al., 2013). Bouguer anomaly maps (Ayala et al., 2016) show that to the south of these faults, the crustal root is deeper, suggesting that the faults are rooted in crustal thickness transition zones. Therefore, they may accommodate the isostatic disequilibrium between contiguous crustal blocks (Fig. 10 and Table 1). This model is also supported by local studies in the westernmost part, suggesting up to 2 mm/yr N-S stretching of the region (Asensio et al., 2012).

In the easternmost Pyrenees, σ_1 rotates into a horizontal N-S orientation (Fig. 5), pointing to a compression subparallel to the regional stress, coherent with the lack of normal faults, in contrast to the western Pyrenees. This phenomenon can be explained by the absence of lithospheric crustal root in the eastern Pyrenees (Gunnell et al., 2008). During the late Oligocene-middle Miocene, the northeastern Iberia underwent extension and thinning due to the opening of the Gulf of Lyon and the Valencia Trough (Roca and Guimerà 1992). In fact, according to Fillon et al. (2021), exhumation in the eastern part of the Pyrenees occurred before 20 Ma, opposite to the ongoing exhumation in the western part. The thinning probably removed totally the crustal root of the eastern Pyrenees. Consequently, the region may have already reached isostatic equilibrium and is primarily undergoing deformation in response to the regional compression.

The Northeastern Iberian margin, located to the south, experiences similar geological history of the easternmost Pyrenees. However, the stress regime along the Iberian Range shows stress ellipsoids with inclined σ_1 and σ_2, and horizontal σ_3 (Fig. 5). The stress field and the normal to strike-slip character of the FMSs (Fig. 10 and Table 1) could result from a combination of extensional processes related to post-rift thermal subsidence experienced since the middle Miocene (Roca and Guimerà 1992) and regional compression. Associated with thermal subsidence, the area between the Iberian Range and the Catalonian Coastal Ranges undergoes relative uplift (Simón, 1982; Scotti et al., 2014), explaining the radial distribution of the normal faults (Peiro, 2023). In addition, this process could be accentuated by the slow gravitational dismantling of the mentioned mountain ranges.

In the High Atlas, surface deformation is also minimal, with shortening rates of less than 0.5 mm/yr, as reported previously (Koulali et al., 2011; Chalouan et al., 2023). This low shortening contrasts with moderate-to-high magnitude earthquakes for which estimated FMSs reveal active thrust and strike-slip faulting (Udías et al., 1989; Cheloni et al., 2024), which operate under a NW-SE compressional regime (Fig. 5). Moreover, the High Atlas is characterized by the highest elevations in the study area, reaching 4000 m above sea level. Surprisingly, gravimetric and seismic data (Teixell et al., 2005; Fullea et al., 2007; Miller and Becker, 2014) and magnetotelluric studies (Anahnah et al., 2011) show the absence of a significant crustal root beneath the High Atlas, and the presence of an anomalous mantle. Therefore, the presence of ascending mantle dome is proposed to explain the elevation. This phenomenon would imply an increase in vertical stress (σ_V), which contrasts with the subvertical values of σ_3. In this context, the NW-SE compression due to the Eurasia-Africa convergence is necessary to orient σ_1 in a NW-SE direction. Thus, though NW-SE compression seems to be significant, the region undergoes low shortening and uplift driven by mantle upwelling (Fig. 10 and Table 1). This context favors the low slip-rates of faults and earthquake long-recurrence periods that could explain the relative lower seismicity in the region.

6. Conclusions

We present the first integrated stress and strain-rate fields for Iberia and Northwestern Africa, derived from a) newly compiled earthquake focal mechanism catalog, and b) an updated GNSS velocity field. Key findings reveal that most of the Eurasia-Africa convergence in this region is accommodated across the plate boundary zone, with particular emphasis on the control of the Gibraltar Arc and the Alboran Domain on strain partitioning.

Based on stress–strain patterns and the crustal types involved, the following sectors are defined: a) the *Atlantic sector*, characterized by direct lithospheric interaction between the Eurasia and Africa, and three mediterranean sectors, b) the *Gibraltar sector*, comprising the westward displacing western Gibraltar Arc, c) the *Alboran sector*, where the shortening is localized in the Alboran thinned continental crust, and d) the *Algero-Balearic sector*, featuring the strong Algero-Balearic oceanic crust between Iberia and Africa.

The spatial variation in boundary conditions and the angular relations between South Iberian margin and Eurasia-Africa convergence likely contribute to the clockwise rotation of Iberia. The Atlantic sector is characterized by an oblique convergence and direct Eurasia-Africa lithospheric coupling, facilitating the stresses to be transmitted to Iberia. On the other hand, the convergence in the Mediterranean is perpendicular to the Iberian margin and is mostly accommodated along the Alboran Domain and detached margins.

The tectonic evolution of interior regions in Iberia and Northwestern Africa is primarily governed by regional compression, as exemplified by W Iberia. However, additional geodynamic processes significantly modulate deformation patterns: a) in the western Pyrenees, isostatic rebound drives normal fault activity, b) NE Iberia experiences *trans*-pressive deformation resulting from the combined effects of thermal subsidence and far-field compressive stresses, and c) both the regional compression and mantle upwelling determines the thrusting in the High Atlas.

This study demonstrates the power of the multidisciplinary, grid-based, stress–strain analysis to unravel complex seismotectonic patterns across extensive plate boundary zones. This integrated approach proves particularly valuable for deciphering the intricate geodynamic processes along the Eurasia-Africa plate boundary in the Atlantic-Mediterranean transition zone.

CRediT authorship contribution statement

Asier Madarieta-Txurruka: Writing – original draft, Visualization, Methodology, Investigation, Formal analysis, Data curation, Conceptualization. **Juan F. Prieto:** Writing – review & editing, Data curation. **Joaquín Escayo:** Writing – review & editing, Data curation. **Federico Pietrolungo:** Writing – review & editing, Software, Methodology, Investigation, Formal analysis. **José A. Peláez:** Writing – review & editing, Validation, Data curation. **Jesús Galindo-Zaldívar:** Writing – review & editing, Validation, Supervision, Funding acquisition, Conceptualization. **Jesús Henares:** Writing – review & editing, Data curation. **Federica Sparacino:** Writing – review & editing, Data curation. **Gemma Ercilla:** Writing – review & editing, Funding acquisition. **José Fernández:** Writing – review & editing, Validation, Resources, Funding acquisition. **Mimmo Palano:** Writing – review & editing, Validation, Supervision, Software, Resources, Project administration, Methodology, Investigation, Funding acquisition, Formal analysis, Data curation, Conceptualization.

Declaration of competing interest

The authors declare that they have no known competing financial interests or personal relationships that could have appeared to influence the work reported in this paper.

Acknowledgments

We are grateful to Dr. A. Vasanthi for handling the editorial process of the manuscript and to the anonymous reviewers for their constructive comments, which greatly helped to improve the quality of the article. This work has been supported by the IT-1678/22 research group of the Basque Government and RNM-148 and RNM-370 research groups of Junta de Andalucía; and PID2022-136678NB-I00 financed by MICIU/AEI 10.13039/501100011033 and FEDER, UE; and by Grant G2HOT-SPOTS (PID2021-122142OBI00) from the AEI/10.13039/501100011033/Union EuropeaNextGenerationEU/PRTR. A.M.T. is supported by the postdoctoral contract funded by the "Departamento de Educación del Gobierno Vasco" (Spain) (POS_2023_1_0001). Open Access funding provided by University of Basque Country.

Appendix A. Supplementary data

Supplementary data to this article can be found online at https://doi.org/10.1016/j.gr.2025.08.020.

Data availability

The DTM used in the figures is obtained from the General Bathymetric Chart of the Oceans (https://www.gebco.net/). The historical earthquake databases comprise The European-Mediterranean Earthquake Catalogue (https://doi.org/10.5880/GFZ.EMEC.2021.001) and the SHARE European Earthquake Catalogue (https://www.emidius.eu/SHEEC/) as well as other sources available at Supplementary Table S1. The active faults databases considered here are available at QAFI (https://info.igme.es/qafi/) and GEM (https://www.globalquakemodel.org/product/active-faults-database). The earthquake focal mechanism solutions catalog is completed by the databases available at Global Centroid Moment Tensor Catalog (https://www.globalcmt.org/CMTsearch.html), European-Mediterranean Regional Centroid-Moment Tensors Catalog (https://rcmt2.bo.ingv.it/), Instituto Geográfico Nacional (https://www.ign.es/web/en/ign/portal/tensor-momento-sismico), Instituto Andaluz de Geofísica (https://iagpds.ugr.es/investigacion/proyectos/moment-tensor-catalogue), and International Seismological Centre (https://www.isc.ac.uk/iscbulletin/search/fmechanisms/), and by other sources available at

Supplementary Table S2. The RINEX files of GNSS sites of public networks of Spain, France, Portugal and regional administrations are available in the databases provided in Supplementary Table S4. The RINEX files of the episodic measurements in Morocco are available in the UNAVCO archive (https://www.unavco.org).

References

Aki, K., Richards, P.G., 2002. Quantitative Seismology. W.H. Freeman and Company, San Francisco, CA.

Altamimi, Z., Métivier, L., Rebischung, P., Rouby, H., Collilieux, X., 2017. ITRF2014 plate motion model. Geophys. J. Int. 209 (3), 1906–1912. https://doi.org/10.1093/gji/ggx136.

Alves, T.M., 2024. Networks of geometrically coherent faults accommodate Alpine tectonic inversion offshore southwestern Iberia. Solid Earth 15 (1), 39–62. https://doi.org/10.5194/se-15-39-2024.

Anahnah, F., Galindo-Zaldívar, J., Chalouan, A., Pedrera, A., Ruano, P., Pous, J., Heise, W., Ruiz-Constán, A., Benmakhlouf, M., López-Garrido, A.C., Ahmamou, M., Sanz de Galdeano, C., Arzate, J., Ibarra, P., González-Castillo, L., Bouregba, N., Corbo, F., Asensio, E., 2011. Deep resistivity cross section of the intraplate Atlas Mountains (NW Africa): New evidence of anomalous mantle and related Quaternary volcanism. Tectonics 30 (5), TC5009. https://doi.org/10.1029/2010TC002859.

Anderson, E.M., 1905. The dynamics of faulting. Trans. Edinb. Geol. Soc. 8 (3), 387–402.

Angrand, P., Mouthereau, F., Masini, E., Asti, R., 2020. A reconstruction of Iberia accounting for Western Tethys-North Atlantic kinematics since the late-Permian-Triassic. Solid Earth 11 (4), 1313–1332. https://doi.org/10.5194/se-11-1313-2020.

Arboleya, M.L., Teixell, A., Charroud, M., Julivert, M., 2004. A structural transect through the High and Middle Atlas of Morocco. J. Afr. Earth Sci. 39 (3–5), 319–327. https://doi.org/10.1016/j.jafrearsci.2004.07.036.

Arche, A., López-Gómez, J., 1996. Origin of the Permian-Triassic Iberian basin, central-eastern Spain. Tectonophysics 266 (1–4), 443–464. https://doi.org/10.1016/S0040-1951(96)00202-8.

Asensio, E., Khazaradze, G., Echeverría, A., King, R.W., Vilajosana, I., 2012. GPS studies of active deformation in the Pyrenees. Geophys. J. Int. 190 (2), 913–921. https://doi.org/10.1111/j.1365-246X.2012.05525.x.

Aurell, M., Fregenal-Martínez, M., Bádenas, B., Muñoz-García, M.B., Élez, J., Meléndez, N., De Santisteban, C., 2019. Middle Jurassic-Early Cretaceous tectono-sedimentary evolution of the southwestern Iberian Basin (central Spain). Earth-Sci. Rev. 199, 102983. https://doi.org/10.1016/j.earscirev.2019.102983.

Ayala, C., Bohoyo, F., Maestro, A., Reguera, M.I., Torne, M., Rubio, F., Fernández, M., García-Lobón, J.L., 2016. Updated Bouguer anomalies of the Iberian Peninsula: a new perspective to interpret the regional geology. J. Maps 12 (5), 1089–1092. https://doi.org/10.1080/17445647.2015.1126538.

Balfour, N.J., Savage, M.K., Townend, J., 2005. Stress and crustal anisotropy in Marlborough, New Zealand: evidence for low fault strength and structure-controlled anisotropy. Geophys. J. Int. 163 (3), 1073–1086. https://doi.org/10.1111/j.1365-246X.2005.02783.x.

Balfour, N.J., Cassidy, J.F., Dosso, S.E., Mazzotti, S., 2011. Mapping crustal stress and strain in southwest British Columbia. J. Geophys. Res. Solid Earth 116 (B3). https://doi.org/10.1029/2010JB008003.

Baptista, M.A., Miranda, J.M., Batlló, J., 2014. The 1531 Lisbon earthquake: a tsunami in the Tagus Estuary? Bull. Seismol. Soc. Am. 104 (5), 2149–2161. https://doi.org/10.1785/0120130316.

Baptista, M.A., Miranda, P.M.A., Miranda, J.M., Victor, L.M., 1998. Constrains on the source of the 1755 Lisbon tsunami inferred from numerical modelling of historical data. J. Geodyn. 25 (1–2), 159–174. https://doi.org/10.1016/S0264-3707(97)00020-3.

Berberian, M., 1995. Master "blind" thrust faults hidden under the Zagros folds: active basement tectonics and surface morphotectonics. Tectonophysics 241 (3–4), 193–224. https://doi.org/10.1016/0040-1951(94)00185-C.

Bezzeghoud, M., Dimitro, D., Ruegg, J.C., Lammali, K., 1995. Faulting mechanism of the El Asnam (Algeria) 1954 and 1980 earthquakes from modelling of vertical movements. Tectonophysics 249, 249–266. https://doi.org/10.1016/0040-1951(95)00032-I.

Billi, A., Cuffaro, M., Orecchio, B., Palano, M., Presti, D., Totaro, C., 2023. Retracing the Africa-Eurasia nascent convergent boundary in the Western Mediterranean based on earthquake and GNSS data. Earth Planet. Sci. Lett. 601, 117906. https://doi.org/10.1016/j.epsl.2022.117906.

Bird, P., 2003. An updated digital model of plate boundaries. Geochem. Geophys. Geosyst. 4 (3). https://doi.org/10.1029/2001GC000252.

Bird, P., Ben-Avraham, Z., Schubert, G., Andreoli, M., Viola, G., 2006. Patterns of stress and strain-rate in southern Africa. J. Geophys. Res. Solid Earth 111 (B8). https://doi.org/10.1029/2005JB003882.

Booth-Rea, G., Azañón, J.M., Azor, A., García-Dueñas, V., 2004. Influence of strike-slip fault segmentation on drainage evolution and topography. A case study: the Palomares Fault Zone (southeastern Betics, Spain). J. Struct. Geol. 26 (9), 1615–1632. https://doi.org/10.1016/j.jsg.2004.01.007.

Borque, M.J., Sánchez-Alzola, A., Martín-Rojas, I., Alfaro, P., Molina, S., Rosa-Cintas, S., Rodríguez-Caderot, G., de Lacy, C., García-Armenteros, J.A., Avilés, M., Herrera-Olmo, A., García-Tortosa, F.J., Estévez, A., Gil, A.J., 2019. How much Nubia-Eurasia convergence is accommodated by the NE end of the Eastern Betic Shear Zone (SE Spain)? Constraints from GPS velocities. Tectonics 38 (5), 1824–1839. https://doi.org/10.1029/2018TC004970.

Bott, M.H.P., 1959. The mechanics of oblique slip faulting. Geol. Mag. 96 (2), 109–117. https://doi.org/10.1017/S0016756800059987.

Bougrine, A., Yelles-Chaouche, A.K., Calais, E., 2019. Active deformation in Algeria from continuous GPS measurements. Geophys. J. Int. 217 (1), 572–588. https://doi.org/10.1093/gji/ggz035.

Bouhadad, Y., 2001. The Murdjadjo, Western Algeria, fault-related fold: implications for seismic hazard. J. Seismol. 5 (4), 541–558. https://doi.org/10.1023/A:1012039900248.

Bouillin, J.P., Durand-Delga, M., Olivier, P., 1986. Betic-Rifian and Tyrrhenian arcs: distinctive features, genesis and development stages. Dev. Geotecton. 21, 281–304. https://doi.org/10.1016/B978-0-444-42688-8.50017-5.

Braga, J.C., Martín, J.M., Quesada, C., 2003. Patterns and average rates of late Neogene–Recent uplift of the Betic Cordillera, SE Spain. Geomorphology 50 (1–3), 3–26. https://doi.org/10.1016/S0169-555X(02)00205-2.

Braunmiller, J., Kradolfer, U., Baer, M., Giardini, D., 2002. Regional moment tensor determination in the European–Mediterranean area—initial results. Tectonophysics 356 (1–3), 5–22. https://doi.org/10.1016/S0040-1951(02)00374-8.

Buforn, E., Udías, A., Colombas, M.A., 1988. Seismicity, source mechanisms and tectonics of the Azores-Gibraltar plate boundary. Tectonophysics 152 (1–2), 89–118. https://doi.org/10.1016/0040-1951(88)90031-5.

Cabral, J., 2012. Neotectonics of mainland Portugal: state of the art and future perspectives. J. Iberian Geol. 38 (1), 71–84. https://doi.org/10.5209/rev_JIGE.2012.v38.n1.39206.

Cabral, J., Mendes, V.B., Figueiredo, P., da Silveira, A.B., Pagarete, J., Ribeiro, A., Dias, R., Ressurreição, R., 2017. Active tectonics in Southern Portugal (SW Iberia) inferred from GPS data. J. Geodyn. 112, 1–11. https://doi.org/10.1016/j.jog.2017.10.002.

Cabral, J., Moniz, C., Batlló, J., Figueiredo, P., Carvalho, J., Matias, L., Teves-Costa, P., Días, R., Simão, N., 2013. The 1909 Benavente (Portugal) earthquake: search for the source. Nat. Hazards 69, 1211–1227. https://doi.org/10.1007/s11069-011-0062-8.

Calais, E., DeMets, C., Nocquet, J.M., 2003. Evidence for a post-3.16-Ma change in Nubia–Eurasia–North America plate motions? Earth Planet. Sci. Lett. 216 (1–2), 81–92. https://doi.org/10.1016/S0012-821X(03)00482-5.

Carmona, E., Stich, D., Ibañez, J.M., Saccorotti, G., 2009. Multiplet focal mechanisms from polarities and relative locations: the Iznajar swarm in southern Spain. Bull. Seismol. Soc. Am. 99 (6), 3421–3429. https://doi.org/10.1785/0120090036.

Carvalho, J., Pinto, C., Dias, R., Rabeh, T., Torres, L., Borges, J., Torres, R., Duarte, H., 2017. Tectonic evolution of an intraplate basin: the lower Tagus Cenozoic Basin, Portugal. Basin Res. 29 (5), 636–657. https://doi.org/10.1111/bre.12193.

Carvalho, J., Rabeh, T., Bielik, M., Szalaiová, E., Torres, L., Silva, M., Carrilho, F., Marias, L., Miranda, J.M., 2011. Geophysical study of the Ota–VF Xira–Lisbon–Sesimbra fault zone and the lower Tagus Cenozoic basin. J. Geophys. Eng. 8 (3), 395–411. https://doi.org/10.1088/1742-2132/8/3/001.

Chalouan, A., Gil, A.J., Chabli, A., Bargach, K., Liemlahi, H., El Kadiri, K., Tendero-Salmerón, V., Galindo-Zaldívar, J., 2023. cGPS record of active extension in Moroccan Meseta and shortening in atlasic chains under the Eurasia-Nubia convergence. Sensors 23 (10), 4846. https://doi.org/10.3390/s23104846.

Cheloni, D., Famiglietti, N.A., Tolomei, C., Caputo, R., Vicari, A., 2024. The 8 September 2023, MW 6.8, Morocco earthquake: A deep transpressive faulting along the active high Atlas mountain belt. Geophys. Res. Lett. 51(2), e2023GL106992. Doi: 10.1029/2023GL106992.

Chiarabba, C., Palano, M., 2017. Progressive migration of slab break-off along the southern Tyrrhenian plate boundary: Constraints for the present day kinematics. J. Geodyn. 105, 51–61. https://doi.org/10.1016/j.jog.2017.01.006.

Civiero, C., Custódio, S., Duarte, J.C., Mendes, V.B., Faccenna, C., 2020. Dynamics of the Gibraltar arc system: a complex interaction between plate convergence, slab pull, and mantle flow. J. Geophys. Res. Solid Earth 125 (7), e2019JB018873. https://doi.org/10.1029/2019JB018873.

Coppier, G., Griveaud, P., de Larouziere, F.D., Montenat, C., Ott d'Estevou, P., 1989. Example of neogene tectonic indentation in the eastern betic cordilleras: the Arc of Aguilas (Southeastern Spain). Geodin. Acta 3 (1), 37–51. https://doi.org/10.1080/09853111.1989.11105173.

Costa, C.H., Gardini, C.E., Diederix, H., Cortés, J.M., 2000. The andean orogenic front at sierra de Las peñas-las Higueras, Mendoza, Argentina. J. South Am. Earth Sci. 13 (3), 287–292. https://doi.org/10.1016/S0895-9811(00)00010-9.

Custódio, S., Dias, N.A., Carrilho, F., Góngora, E., Rio, I., Marreiros, C., Morais, I., Alves, P., Matias, L., 2015. Earthquakes in western Iberia: improving the understanding of lithospheric deformation in a slowly deforming region. Geophys. J. Int. 203 (1), 127–145. https://doi.org/10.1093/gji/ggv285.

de Vicente, G.D., Cloetingh, S.A.P.L., Muñoz-Martín, A., Olaiz, A., Stich, D., Vegas, R., Galindo-Zaldívar, J., Fernández-Lozano, J., 2008. Inversion of moment tensor focal mechanisms for active stresses around the microcontinent Iberia: tectonic implications. Tectonics 27 (1), TC1008. https://doi.org/10.1029/2006TC002093.

de Vicente, G., Cunha, P.P., Muñoz-Martín, A., Cloetingh, S.A.P.L., Olaiz, A., Vegas, R., 2018. The Spanish-Portuguese Central System: an example of intense intraplate deformation and strain partitioning. Tectonics 37 (12), 4444–4469. https://doi.org/10.1029/2018TC005204.

de Vicente, G., Vegas, R., Muñoz-Martín, A., Van Wees, J.D., Casas-Sáinz, A., Sopeña, A., Sánchez-Moya, Y., Arche, A., López-Gómez, J., Olaiz, A., Fernández-Lozano, J., 2009. Oblique strain partitioning and transpression on an inverted rift: the Castilian Branch of the Iberian Chain. Tectonophysics 470 (3–4), 224–242. https://doi.org/10.1016/j.tecto.2008.11.003.

Druet, M., Bohoyo, F., Maestro, A., Mink, S., García-Senz, J., Pedrera, A., Rodríguez Fernández, R., 2023. Tectonics of the Iberian continental margins and abyssal plains. J. Maps 19 (1), 2237980. https://doi.org/10.1080/17445647.2023.2237980.

Duarte, J.C., Riel, N., Rosas, F.M., Popov, A., Schuler, C., Kaus, B.J., 2024. Gibraltar subduction zone is invading the Atlantic. Geology 52 (5), 331–335. https://doi.org/10.1130/G51654.1.
Echeverría, A., Khazaradze, G., Asensio, E., Masana, E., 2015. Geodetic evidence for continuing tectonic activity of the Carboneras fault (SE Spain). Tectonophysics 663, 302–309. https://doi.org/10.1016/j.tecto.2015.08.009.
Echeverría, A., Khazaradze, G., Asensio, E., Gárate, J., Dávila, J.M., Suriñach, E., 2013. Crustal deformation in eastern Betics from CuaTeNeo GPS network. Tectonophysics 608, 600–612. https://doi.org/10.1016/j.tecto.2013.08.020.
Ercilla, G., Galindo-Zaldívar, J., Estrada, F., Valencia, J., Juan, C., Casas, D., Alonso, B., Comas, M.C., Tendero-Salmerón, V., Casalbore, D., Azpiroz-Zabala, M., Bárcenas, P., Ceramicola, S., Chiocci, F.L., Idárraga-García, J., López-González, N., Mata, P., Palomino, D., Rodríguez-García, J.A., Teixeira, M., Yenes, M., 2022. Understanding the complex geomorphology of a deep sea area affected by continental tectonic indentation: the case of the Gulf of Vera (Western Mediterranean). Geomorphology 402, 108126. https://doi.org/10.1016/j.geomorph.2022.108126.
Ercilla, G., Galindo-Zaldívar, J., Juan, C., Estrada, F., Iglesias, J., Valencia, J., Tendero-Salmerón, V., d'Acremont, E., Fernández-Puga, M.C., González-Castillo, L., Madarieta-Txurruka, A., Palomino, D., Teixeira, M., Vázquez, J.T., 2025. Geomorphology of the northern and southern continental margins of the Iberian Peninsula: quaternary interplay of tectonics and sedimentation. Mar. Geol., 107467 https://doi.org/10.1016/j.margeo.2024.107467.
Estrada, F., Galindo-Zaldívar, J., Vázquez, J.T., Ercilla, G., d'Acremont, E., Alonso, B., Gorini, C., 2018. Tectonic indentation in the central Alboran Sea (westernmost Mediterranean). Terra Nova 30 (1), 24–33. https://doi.org/10.1111/ter.12304.
Fadil, A., Vernant, P., McClusky, S., Reilinger, R., Gómez, F., Ben Sari, D., Mourabir, T., Feigl, K., Barazangi, M., 2006. Active tectonics of the western Mediterranean: Geodetic evidence for rollback of a delaminated subcontinental lithospheric slab beneath the Rif Mountains, Morocco. Geology 34 (7), 529–532. https://doi.org/10.1130/G22291.1.
Fang, P., Tugend, J., Mohn, G., Kusznir, N., Ding, W., 2021. Evidence for rapid large-amplitude vertical motions in the Valencia Trough (Western Mediterranean) generated by 3D subduction slab roll-back. Earth Planet. Sci. Lett. 575, 117179. https://doi.org/10.1016/j.epsl.2021.117179.
Fernandes, R.M.S., Miranda, J.M., Meijninger, B.M.L., Bos, M.S., Noomen, R., Bastos, L., Ambrosius, B.A.C., Riva, R.E.M., 2007. Surface velocity field of the Ibero-Maghrebian segment of the Eurasia-Nubia plate boundary. Geophys. J. Int. 169 (1), 315–324. https://doi.org/10.1111/j.1365-246X.2006.03252.x.
Fernández-Viejo, G., Llana-Fúnez, S., Acevedo, J., López-Fernández, C., 2021. The Cantabrian fault at sea. Low magnitude seismicity and its significance within a stable setting. Front. Earth Sci. 9, 645061. https://doi.org/10.3389/feart.2021.645061.
Fillon, C., Mouthereau, F., Calassou, S., Pik, R., Bellahsen, N., Gautheron, C., Stockli, D., Brichau, S., Daril, N., Mouchené, M., van der Beek, P., 2021. Post-orogenic exhumation in the western Pyrenees: evidence for extension driven by pre-orogenic inheritance. J. Geol. Soc. 178 (2), jgs2020-079. https://doi.org/10.1144/jgs2020-079.
Flesch, L.M., Holt, W.E., Haines, A.J., Shen-Tu, B., 2000. Dynamics of the Pacific-North American plate boundary in the western United States. Science 287 (5454), 834–836. https://doi.org/10.1126/science.287.5454.834.
Frizon de Lamotte, D., Saint Bezar, B., Bracène, R., Mercier, E., 2000. The two main steps of the Atlas building and geodynamics of the western Mediterranean. Tectonics 19 (4), 740–761. https://doi.org/10.1029/2000TC900003.
Frohlich, C., 1992. Triangle diagrams: ternary graphs to display similarity and diversity of earthquake focal mechanisms. Phys. Earth Planet. Inter. 75 (1–3), 193–198. https://doi.org/10.1016/0031-9201(92)90130-N.
Fonseca, J.F., Palano, M., Falcão, A.P., Hrysiewicz, A., Fernandez, J., 2021. Interseismic strain accumulation near Lisbon (Portugal) from space geodesy. Geophys. Res. Lett. 48 (24), e2021GL096862. https://doi.org/10.1029/2021GL096862.
Fullea, J., Fernàndez, M., Zeyen, H., Vergés, J., 2007. A rapid method to map the crustal and lithospheric thickness using elevation, geoid anomaly and thermal analysis. Application to the Gibraltar Arc System, Atlas Mountains and adjacent zones. Tectonophysics 430 (1–4), 97–117. https://doi.org/10.1016/j.tecto.2006.11.003.
Galindo-Zaldívar, J., Ercilla, G., Estrada, F., Catalán, M., d'Acremont, E., Azzouz, O., Casas, D., Chourak, M., Vázquez, J.T., Chalouan, A., Sanz de Galdeano, J., Benmakhlouf, M., Gorini, C., Alonso, B., Palomino, B., Rengel, J.A., Gil, A.J., 2018. Imaging the growth of recent faults: the case of 2016–2017 seismic sequence sea bottom deformation in the Alboran Sea (Western Mediterranean). Tectonics 37 (8), 2513–2530. https://doi.org/10.1029/2017TC004941.
Galindo-Zaldívar, J., Maldonado, A., Schreider, A.A., 2003. Gorringe Ridge gravity and magnetic anomalies are compatible with thrusting at a crustal scale. Geophys. J. Int. 153 (3), 586–594. https://doi.org/10.1046/j.1365-246X.2003.01922.x.
Galindo-Zaldívar, J., Gil, A.J., Sanz de Galdeano, C., Lacy, M.C., García-Armenteros, J.A., Ruano, P., Ruiz, A.M., Martínez-Martos, M., Alfaro, P., 2015. Active shallow extension in central and eastern Betic Cordillera from CGPS data. Tectonophysics 663, 290–301. https://doi.org/10.1016/j.tecto.2015.08.035.
Galindo-Zaldívar, J., Gil, A.J., Tendero-Salmerón, V., Borque, M.J., Ercilla, G., González-Castillo, L., Sánchez-Alzola, A., de Lacy, M.C., Estrada, F., Avilés, M., Alfaro, P., Madarieta-Txurruka, A., Chacón, F., 2022. The Campo de Dalias GNSS Network Unveils the interaction between roll-back and indentation tectonics in the Gibraltar Arc. Sensors 22 (6), 2128. https://doi.org/10.3390/s22062128.
Galindo-Zaldívar, J., Jabaloy, A., Serrano, I., Morales, J., González-Lodeiro, F., Torcal, F., 1999. Recent and present-day stresses in the Granada Basin (Betic Cordilleras): example of a late Miocene-present-day extensional basin in a convergent plate boundary. Tectonics 18 (4), 686–702. https://doi.org/10.1029/1999TC900016.
Garate, J., Martin-Davila, J., Khazaradze, G., Echeverría, A., Asensio, E., Gil, A.J., de Lacy, M.C., Armenteros, J.A., Ruiz, A.M., Gallastegui, J., Alvarez-Lobato, F., Ayala, C., Rodríguez-Caderot, G., Galindo-Zaldívar, J., Rimi, A., Harnafi, M., 2015. Topo-Iberia project: CGPS crustal velocity field in the Iberian Peninsula and Morocco. GPS Solut. 19, 287–295. https://doi.org/10.1007/s10291-014-0387-3.
García-Mayordomo, J., Martín-Banda, R., 2022. Guide for the Use of QAFI v. 4. Instituto Geológico y Minero de España (IGME), CSIC, Madrid. https://info.igme.es/qafi/docs/QAFI_v4_Guide.pdf.
Gea, P.J., Negredo, A.M., Mancilla, F.D.L., 2023. The Gibraltar slab dynamics and its influence on past and present-day Alboran domain deformation: Insights from thermo-mechanical numerical modelling. Front. Earth Sci. 11, 995041. https://doi.org/10.3389/feart.2023.995041.
Gómez de la Peña, L., Ranero, C.R., Gràcia, E., Booth-Rea, G., Azañón, J.M., Tinivella, U., Yelles-Chaouche, A., 2022. Evidence for a developing plate boundary in the western Mediterranean. Nat. Commun. 13 (1), 4786. https://doi.org/10.1038/s41467-022-31895-z.
Gómez de la Peña, L., Ranero, C.R., Gràcia, E., 2018. The crustal domains of the Alboran Basin (western Mediterranean). Tectonics 37 (10), 3352–3377. https://doi.org/10.1029/2017TC004946.
Gomez, F., Barazangi, M., Bensaid, M., 1996. Active tectonism in the intracontinental Middle Atlas Mountains of Morocco: synchronous crustal shortening and extension. J. Geol. Soc. 153 (3), 389–402. https://doi.org/10.1144/gsjgs.153.3.0389.
González-Castillo, L., Galindo-Zaldívar, J., de Lacy, M.C., Borque, M.J., Martínez-Moreno, F.J., García-Armenteros, J.A., Gil, A.J., 2015a. Active rollback in the Gibraltar Arc: evidences from CGPS data in the western Betic Cordillera. Tectonophysics 663, 310–321. https://doi.org/10.1016/j.tecto.2015.03.010.
González-Castillo, L., Galindo-Zaldívar, J., Pedrera, A., Martínez-Moreno, F.J., Ruano, P., 2015b. Shallow frontal deformation related to active continental subduction: structure and recent stresses in the westernmost Betic Cordillera. Terra Nova 27 (2), 114–121. https://doi.org/10.1111/ter.12138.
Gràcia, E., Danobeitia, J., Vergés, J., Bartolomé, R., Córdoba, D., 2003. Crustal architecture and tectonic evolution of the Gulf of Cadiz (SW Iberian margin) at the convergence of the Eurasian and African plates. Tectonics 22 (4), 1033. https://doi.org/10.1029/2001TC901045.
Grevemeyer, I., Gràcia, E., Villaseñor, A., Leuchters, W., Watts, A.B., 2015. Seismicity and active tectonics in the Alboran Sea, Western Mediterranean: constraints from an offshore-onshore seismological network and swath bathymetry data. J. Geophys. Res. Solid Earth 120 (12), 8348–8365. https://doi.org/10.1002/2015JB012073.
Grünthal, G., Wahlström, R., 2012. The European-Mediterranean earthquake catalogue (EMEC) for the last millennium. J. Seismol. 16, 535–570. https://doi.org/10.1007/s10950-012-9302-y.
Gunnell, Y., Zeyen, H., Calvet, M., 2008. Geophysical evidence of a missing lithospheric root beneath the Eastern Pyrenees: consequences for post-orogenic uplift and associated geomorphic signatures. Earth Planet. Sci. Lett. 276 (3–4), 302–313. https://doi.org/10.1016/j.epsl.2008.09.031.
Gutiérrez, F., 2012. A review on Quaternary tectonic and nontectonic faults in the central sector of the Iberian Chain, NE Spain. J. Iberian Geol. 38 (1), 145–160. https://doi.org/10.5209/rev_JIGE.2012.v38.n1.39210.
Gutscher, M.A., 2004. What caused the great Lisbon earthquake? Science 305 (5688), 1247–1248. https://doi.org/10.1126/science.1101351.
Hamdache, M., Peláez, J.A., Yelles-Chauche, A.K., 2004. The Algiers, Algeria Earthquake (Mw 6.8) of 21 May 2003: preliminary report. Seismol. Res. Lett. 75 (3), 360–367. https://doi.org/10.1785/gssrl.75.3.360.
Hamdache, M., Peláez, J.A., Gospodinov, D., Henares, J., Galindo Zaldívar, J., Sanz de Galdeano, C., Ranguelov, B., 2022. Stochastic modeling of the Al Hoceima (Morocco) aftershocks sequences of 1994, 2004 and 2016. Appl. Sci. 12, 8744. https://doi.org/10.3390/app12178744.
Hamdache, M., Peláez, J.A., Talbi, A., López Casado, C., 2010. A unified catalog of main earthquakes for Northern Algeria from A.D. 856 to 2008. Seismol. Res. Lett. 81, 732–739. https://doi.org/10.1785/gssrl.81.5.732.
Heidbach, O., Rajabi, M., Cui, X., Fuchs, K., Müller, B., Reinecker, J., Reiter, K., Tingay, M., Wenzel, F., Xie, F., Ziegler, M.O., Zoback, M.L., Zoback, M., 2018. The World Stress Map database release 2016: crustal stress pattern across scales. Tectonophysics 744, 484–498. https://doi.org/10.1016/j.tecto.2018.07.007.
Henares, J., Hamdache, M., Peláez, J.A., Sanz de Galdeano, C., López Casado, C., 2024. Multitemporal analysis of seismicity of the Trans-Alboran shear zone. Phys. Chem. Earth 134, 103557. https://doi.org/10.1016/j.pce.2024.103557.
Herraiz, M., de Vicente, G.D., Lindo-Ñaupari, R., Giner, J., Simón, J.L., González-Casado, J.M., Vadillo, O., Rodríguez-Pascua, M.A., Cicuéndez, J.I., Casas, A., Cabañas, L., Rincón, P., Cortés, A.L., Ramírez, M., Lucini, M., 2000. The recent (upper Miocene to Quaternary) and present tectonic stress distributions in the Iberian Peninsula. Tectonics 19 (4), 762–786. https://doi.org/10.1029/2000TC900006.
Herring, T.A., King, R.W., Floyd, M.A., McClusky, S.C., 2017. Introduction to GAMIT/GLOBK, Release 10.7. Massachusetts Institute of Technology. http://geoweb.mit.edu/gg/Intro_GG.pdf.
IGN, 2025. Spanish Seismic Catalogue. National Geographic Institute (IGN). https://doi.org/10.7419/162.03.2022.
Jacobshagen, V., Görler, K., Giese, P., 1988. Geodynamic evolution of the Atlas System (Morocco) in post-Palaeozoic times. In: The Atlas System of Morocco: Studies on its Geodynamic Evolution. Springer, pp. 481-499. Doi: 10.1007/BFb0011606.
Jiménez-Munt, I., Fernàndez, M., Torne, M., Bird, P., 2001. The transition from linear to diffuse plate boundary in the Azores-Gibraltar region: results from a thin-sheet model. Earth Planet. Sci. Lett. 192 (2), 175–189. https://doi.org/10.1016/S0012-821X(01)00442-3.
Jolivet, L., Faccenna, C., 2000. Mediterranean extension and the Africa-Eurasia collision. Tectonics 19 (6), 1095–1106. https://doi.org/10.1029/2000TC900018.

Jolivet, L., Augier, R., Faccenna, C., Negro, F., Rimmele, G., Agard, P., Robin, C., Rossetti, F., Crespo-Blanc, A., 2008. Subduction, convergence and the mode of backarc extension in the Mediterranean region. Bull. Soc. Géol. Fr. 179 (6), 525–550. https://doi.org/10.2113/gssgfbull.179.6.525.

Keiding, M., Lund, B., Árnadóttir, T., 2009. Earthquakes, stress, and strain along an obliquely divergent plate boundary: Reykjanes Peninsula, southwest Iceland. J. Geophys. Res. Solid Earth 114 (B9), B09306. https://doi.org/10.1029/2008JB006253.

Koulali, A., Ouazar, D., Tahayt, A., King, R.W., Vernant, P., Reilinger, R.E., McClusky, S., Mourabit, T., Davila, J.M., Amraoui, N., 2011. New GPS constraints on active deformation along the Africa-Iberia plate boundary. Earth Planet. Sci. Lett. 308 (1–2), 211–217. https://doi.org/10.1016/j.epsl.2011.05.048.

Kreemer, C., Blewitt, G., Klein, E.C., 2014. A geodetic plate motion and Global Strain Rate Model. Geochem. Geophys. Geosyst. 15 (10), 3849–3889. https://doi.org/10.1002/2014GC005407.

Lacan, P., Ortuño Candela, M., 2012. Active tectonics of the Pyrenees: a review. J. Iberian Geol. 38 (1), 9–30. https://doi.org/10.5209/rev_JIGE.2012.v38.n1.39203.

Lachenbruch, A.H., Sass, J.H., 1992. Heat flow from Cajon Pass, fault strength, and tectonic implications. J. Geophys. Res. Solid Earth 97 (B4), 4995–5015. https://doi.org/10.1029/91JB01506.

Laughton, A.S., Whitmarsh, R.B., 1974. The Azores-Gibraltar plate boundary. In: Geodynamics of Iceland and the North Atlantic Area. Springer, Dordrecht, pp. 63–81. https://doi.org/10.1007/978-94-010-2271-2_5.

Levandowski, W., 2023. Fault-slip potential near the deadly 8 September 2023 Mw 6.8 Al Haouz, Morocco. Earthq. Seism. Rec. 3 (4), 367–375. https://doi.org/10.1785/0320230037.

López-Fernández, C., Fernández-Viejo, G., Olona, J., Llana-Fúnez, S., 2018. Intraplate seismicity in northwest Iberia along the trace of the Ventaniella fault: a case for fault intersection at depth. Bull. Seismol. Soc. Am. 108 (2), 604–618. https://doi.org/10.1785/0120170215.

Lund, B., Townend, J., 2007. Calculating horizontal stress orientations with full or partial knowledge of the tectonic stress tensor. Geophys. J. Int. 170 (3), 1328–1335. https://doi.org/10.1111/j.1365-246X.2007.03468.x.

Madarieta-Txurruka, A., Galindo-Zaldívar, J., González-Castillo, L., Peláez, J.A., Ruiz-Armenteros, A.M., Henares, J., Garrido-Carretero, M.S., Avilés, M., Gil, A.J., 2021. High- and low-angle normal fault activity in a collisional orogen: the Northeastern Granada Basin (Betic Cordillera). Tectonics 40 (7), e2021TC006715. https://doi.org/10.1029/2021TC006715.

Madarieta-Txurruka, A., González-Castillo, L., Peláez, J.A., Catalán, M., Henares, J., Gil, A.J., Lamas-Fernández, F., Galindo-Zaldívar, J., 2022. The role of faults as barriers in confined seismic sequences: 2021 seismicity in the Granada Basin (Betic Cordillera). Tectonics 41 (9), e2022TC007481. https://doi.org/10.1029/2022TC007481.

Madarieta-Txurruka, A., González-Castillo, L., Peláez, J.A., Galindo-Zaldívar, J., Borque, M.J., Lacy, M.C., Ruiz-Armenteros, A.M., Henares, J., Ruano, P., Sánchez-Alzola, A., Avilés, M., Rodríguez-Caderot, G., Martínez-Moreno, F.J., Tendero-Salmerón, V., Vinardell-Peña, R., Gil, A.J., 2024. Active shortening simultaneous to normal faulting based on GNSS, geophysical, and geological data: the seismogenic Ventas de Zafarraya Fault (Betic Cordillera, southern Spain). Tectonics 43 (2), e2023TC007956. https://doi.org/10.1029/2023TC007956.

Madarieta-Txurruka, A., Peláez, J.A., González-Castillo, L., Gil, A.J., Galindo-Zaldívar, J., 2023. Active collapse in the central Betic Cordillera: development of the extensional system of the Granada Basin. Appl. Sci. 13 (16), 9138. https://doi.org/10.3390/app13169138.

Maillard, A., Mauffret, A., 1999. Crustal structure and riftogenesis of the Valencia Trough (north-western Mediterranean Sea). Basin Res. 11 (4), 357–379. https://doi.org/10.1046/j.1365-2117.1999.00105.x.

Martínez-García, P., Comas, M., Soto, J.I., Lonergan, L., Watts, A.B., 2013. Strike-slip tectonics and basin inversion in the Western Mediterranean: the Post-Messinian evolution of the Alboran Sea. Basin Res. 25 (4), 361–387. https://doi.org/10.1111/bre.12005.

Martínez-Loriente, S., Gràcia, E., Bartolome, R., Perea, H., Klaeschen, D., Danobeitia, J. J., Zitellini, N., Wynn, R.B., Masson, D.G., 2018. Morphostructure, tectono-sedimentary evolution and seismic potential of the Horseshoe Fault, SW Iberian Margin. Basin Res. 30, 382–400. https://doi.org/10.1111/bre.12225.

Martínez-Loriente, S., Gracia, E., Bartolome, R., Sallarès, V., Connors, C., Perea, H., Lo Iacono, C., Klaeschen, K., Terrinha, P., Danobeitia, J.J., Zitellini, N., 2013. Active deformation in old oceanic lithosphere and significance for earthquake hazard: Seismic imaging of the Coral Patch Ridge area and neighboring abyssal plains (SW Iberian Margin). Geochem. Geophys. Geosyst. 14 (7), 2206–2231. https://doi.org/10.1002/ggge.20173.

Martínez-Loriente, S., Sallarès, V., Gràcia, E., Bartolome, R., Danobeitia, J.J., Zitellini, N., 2014. Seismic and gravity constraints on the nature of the basement in the Africa-Eurasia plate boundary: new insights for the geodynamic evolution of the SW Iberian margin. J. Geophys. Res. Solid Earth 119 (1), 127–149. https://doi.org/10.1002/2013JB010476.

Martínez-Martos, M., Galindo-Zaldívar, J., de Galdeano, C.S., Garcia-Tortosa, F.J., Martínez-Moreno, F.J., Ruano, P., González-Castillo, L., Azanon, J.M., 2017. Latest extension of the Laujar fault in a convergence setting (Sierra Nevada, Betic Cordillera). J. Geodyn. 104, 15–26. https://doi.org/10.1016/j.jog.2016.12.002.

Martínez-Solares, J.M., Arroyo, A.L., Mezcua, J., 1979. Isoseismal map of the 1755 Lisbon earthquake obtained from spanish data. Tectonophysics 53 (3–4), 301–313. https://doi.org/10.1016/0040-1951(79)90075-1.

Martín-González, F., Crespo-Martín, C., Cesca, S., González-Muñoz, S., 2023. Understanding seismicity and seismotectonics in a stable continental region (NW Iberian Peninsula): implications for the nature of intraplate seismicity. Glob. Planet. Change 227, 104177. https://doi.org/10.1016/j.gloplacha.2023.104177.

Martín-Rojas, I., Alfaro, P., Galindo-Zaldívar, J., Borque-Arancón, M.J., García-Tortosa, F.J., Sanz de Galdeano, C., Avilés, M., Sámchez-Alzola, A., González-Castillo, L., Ruano, P., Medina-Cascales, I., Tendero-Salmerón, V., Madarieta-Txurruka, A., Pedrosa-González, M.T., Gil-Cruz, A.J., 2023. Insights of active extension within a collisional orogen from GNSS (Central Betic Cordillera, S Spain). Tectonics 42 (7), e2022TC007723. https://doi.org/10.1029/2022TC007723.

Mauffret, A., 2007. The northwestern (Maghreb) boundary of the Nubia (Africa) plate. Tectonophysics 429 (1–2), 21–44. https://doi.org/10.1016/j.tecto.2006.09.007.

Mazzotti, S., Aubagnac, C., Bollinger, L., Coca Oscanoa, K., Delouis, B., Do Paco, D., Doubre, C., Godano, M., Jomard, H., Larroque, C., Laurendeau, A., Masson, F., Sylvander, M., Trilla, A., 2021. FMHex20: an earthquake focal mechanism database for seismotectonic analyses in metropolitan France and bordering regions. BSGF-Earth Sci. Bull. 192 (1), 10. https://doi.org/10.1051/bsgf/2020049.

McClusky, S., Reilinger, R., Mahmoud, S.B.S.D., Ben Sari, D., Tealeb, A., 2003. GPS constraints on Africa (Nubia) and Arabia plate motions. Geophys. J. Int. 155 (1), 126–138. https://doi.org/10.1046/j.1365-246X.2003.02023.x.

Meghraoui, M., 1991. Blind reverse faulting system associated with the Mont Chenoua-Tipaza earthquake of 29 October 1989 (north-central Algeria). Terra Nova 3 (1), 84–92. https://doi.org/10.1111/j.1365-3121.1991.tb00847.x.

Michael, A.J., 1987. Use of focal mechanisms to determine stress: a control study. J. Geophys. Res. Solid Earth 92 (B1), 357–368. https://doi.org/10.1029/JB092iB01p00357.

Miller, M.S., Becker, T.W., 2014. Reactivated lithospheric-scale discontinuities localize dynamic uplift of the Moroccan Atlas Mountains. Geology 42 (1), 35–38. https://doi.org/10.1130/G34959.1.

Neres, M., Carafa, M.M.C., Fernandes, R.M.S., Matias, L., Duarte, J.C., Barba, S., Terrinha, P., 2016. Lithospheric deformation in the Africa-Iberia plate boundary: improved neotectonic modeling testing a basal-driven Alboran plate. J. Geophys. Res. Solid Earth 121 (9), 6566–6596. https://doi.org/10.1002/2016JB013012.

Ortuño, M., Martí, A., Martín-Closas, C., Jiménez-Moreno, G., Martinetto, E., Santanach, P., 2013. Palaeoenvironments of the Late Miocene Prüedo Basin: implications for the uplift of the Central Pyrenees. J. Geol. Soc. 170 (1), 79–92. https://doi.org/10.1144/jgs2011-121.

Palano, M., 2015. On the present-day crustal stress, strain-rate fields and mantle anisotropy pattern of Italy. Geophys. J. Int. 200 (2), 969–985. https://doi.org/10.1093/gji/ggu451.

Palano, M., Cannavò, F., Ferranti, L., Mattia, M., Mazzella, M.E., 2011. Strain and stress fields in the Southern Apennines (Italy) constrained by geodetic, seismological and borehole data. Geophys. J. Int. 187 (3), 1270–1282. https://doi.org/10.1111/j.1365-246X.2011.05234.x.

Palano, M., González, P.J., Fernández, J., 2013a. Strain and stress fields along the Gibraltar Orogenic Arc: constraints on active geodynamics. Gondwana Res. 23 (3), 1071–1088. https://doi.org/10.1016/j.gr.2012.05.021.

Palano, M., González, P.J., Fernández, J., 2015. The Diffuse Plate boundary of Nubia and Iberia in the Western Mediterranean: crustal deformation evidence for viscous coupling and fragmented lithosphere. Earth Planet. Sci. Lett. 430, 439–447. https://doi.org/10.1016/j.epsl.2015.08.040.

Palano, M., Imprescia, P., Gresta, S., 2013b. Current stress and strain-rate fields across the Dead Sea Fault System: constraints from seismological data and GPS observations. Earth Planet. Sci. Lett. 369, 305–316. https://doi.org/10.1016/j.epsl.2013.03.043.

Palano, M., Pezzo, G., Serpelloni, E., Devoti, R., D'Agostino, N., Gandolfi, S., Sparacino, F., Anderlini, L., Polizzi, L., Tavasci, L., Macini, P., Pietrantonio, G., Riguzzi, F., Antoncecchi, I., Ciccone, F., Rossi, G., Avallone, A., Selvaggi, G., 2020. Geopositioning time series from offshore platforms in the Adriatic Sea. Sci. Data 7 (1), 373. https://doi.org/10.1038/s41597-020-00705-w.

Pedrera, A., García-Senz, J., Peropadre, C., Robador, A., López-Mir, B., Díaz-Alvarado, J., Rodríguez-Fernández, L.R., 2021. The Getxo crustal-scale cross-section: testing tectonic models in the Bay of Biscay-Pyrenean rift system. Earth-Sci. Rev. 212, 103429. https://doi.org/10.1016/j.earscirev.2020.103429.

Pedrera, A., García-Senz, J., Pueyo, E.L., López-Mir, B., Silva-Casal, R., Díaz-Alvarado, J., 2023. Inhomogeneous rift inversion and the evolution of the Pyrenees. Earth-Sci. Rev. 245, 104555. https://doi.org/10.1016/j.earscirev.2023.104555.

Pedrera, A., Ruiz-Constán, A., Galindo-Zaldívar, J., Chalouan, A., De Galdeano, C.S., Marín-Lechado, C., Ruano, P., Benmakhlouf, M., Akil, M., López-Garrido, A.C., Chabli, A., Ahmamou, M., González-Castillo, L., 2011. Is there an active subduction beneath the Gibraltar orogenic arc? Constraints from Pliocene to present-day stress field. J. Geodyn. 52 (2), 83–96. https://doi.org/10.1016/j.jog.2010.12.003.

Pedrera, A., Ruiz-Constán, A., García-Senz, J., Azor, A., Marín-Lechado, C., Ayala, C., Díaz de Neira, J.A., Rodríguez-Fernández, L.R., 2020. Evolution of the South-Iberian paleomargin: from hyperextension to continental subduction. J. Struct. Geol. 138, 104122. https://doi.org/10.1016/j.jsg.2020.104122.

Pedrera, A., Ruiz-Constán, A., Marín-Lechado, C., Galindo-Zaldívar, J., González, A., Peláez, J.A., 2013. Seismic transpressive basement faults and monocline development in a foreland basin (Eastern Guadalquivir, SE Spain). Tectonics 32 (6), 1571–1586. https://doi.org/10.1002/2013TC003397.

Peiro, A., 2023. In: Fallas activas de la Cordillera Ibérica Centro-Oriental. University of Zaragoza, p. 215 (Ph.D. thesis).

Peláez, J.A., Chourak, M., Tadili, B.A., Brahim, L.A., Hamdache, M., Casado, C.L., Solares, J.M., 2007. A catalog of main Moroccan earthquakes from 1045 to 2005. Seismol. Res. Lett. 78 (6), 614–621. https://doi.org/10.1785/gssrl.78.6.614.

Peláez, J.A., 2023. Deadly Morocco quake resulted from Africa's ongoing collision with Europe. Temblor. https://doi.org/10.32858/temblor.321.

Perea, H., Masana, E., Santanach, P., 2012. An active zone characterized by slow normal faults, the northwestern margin of the València trough (NE Iberia): a review. J. Iberian Geol. 38 (1), 31–52. https://doi.org/10.5209/rev_JIGE.2012.v38.n1.39204.

Pietrolungo, F., Lavecchia, G., Madarieta-Txurruka, A., Sparacino, F., Srivastava, E., Cirillo, D., de Nardis, R., Andrenacci, C., Bello, S., Parrino, N., Sulli, A., Palano, M., 2024. Comparison of Crustal stress and strain fields in the Himalaya-Tibet Region: geodynamic implications. Remote Sens. 16 (24), 4765. https://doi.org/10.3390/rs16244765.

Porkoláb, K., Békési, E., Győri, E., Broerse, T., Czecze, B., Kenyeres, A., Tari, G., Wéber, Z., 2025. Present-day stress field, strain-rate field and seismicity of the Pannonian region: overview and integrated analysis. Geol. Soc. Lond. Spec. Publ. 554 (1), SP554-2023. https://doi.org/10.1144/SP554-2023-219.

Portela, J., Staller, A., Béjar-Pizarro, M., Martínez-Díaz, J.J., Álvarez-Gómez, J.A., Khazaradze, G., 2025. New insights on the crustal deformation in the Eastern Betics from densified GNSS data. Tectonics 44 (2), e2024TC008381. https://doi.org/10.1029/2024TC008381.

Pro, C., Buforn, E., Bezzeghoud, M., Udías, A., 2013. The earthquakes of 29 July 2003, 12 February 2007, and 17 December 2009 in the region of Cape Saint Vincent (SW Iberia) and their relation with the 1755 Lisbon earthquake. Tectonophysics 583, 16–27. https://doi.org/10.1016/j.tecto.2012.10.010.

Reinhardt, L.J., Dempster, T.J., Shroder Jr, J.F., Persano, C., 2007. Tectonic denudation and topographic development in the Spanish Sierra Nevada. Tectonics 26 (3), TC3008. https://doi.org/10.1029/2006TC001954.

Rigo, A., Vernant, P., Feigl, K.L., Goula, X., Khazaradze, G., Talaya, J., Morel, L., Nicolas, J., Baize, S., Chéry, J., Sylvander, M., 2015. Present-day deformation of the Pyrenees revealed by GPS surveying and earthquake focal mechanisms until 2011. Geophys. J. Int. 201 (2), 947–964. https://doi.org/10.1093/gji/ggv052.

Roca, E., Guimerà, J., 1992. The Neogene structure of the eastern Iberian margin: structural constraints on the crustal evolution of the Valencia trough (western Mediterranean). Tectonophysics 203 (1–4), 203–218. https://doi.org/10.1016/0040-1951(92)90224-T.

Rodríguez-Fernández, L.R., López-Olmedo, F., Oliveira, J.T., Medialdea, T., Terrinha, P., Matas González, J., Martín-Serrano García, A., Martín Parra, L.M., Rubio Pascual, F., Marín Lechado, C., Montes Santiago, M., Nozal Martín, F., 2015. Mapa Geológico de España y Portugal a escala 1:1.000.000. Instituto Geológico y Minero de España, Laboratório Nacional de Energía e Geología de Portugal, Madrid. https://info.igme.es/cartografiadigital/datos/geologicos1M/Geologico1000_(2015)/pdfs/EditadoG1000_(2015).pdf.

Romagny, A., Jolivet, L., Menant, A., Bessière, E., Maillard, A., Canva, A., Gorini, C., Augier, R., 2020. Detailed tectonic reconstructions of the Western Mediterranean region for the last 35 Ma, insights on driving mechanisms. Bull. Soc. Géol. Fr. 191 (1), 37. https://doi.org/10.1051/bsgf/2020040.

Rosenbaum, G., Lister, G.S., Duboz, C., 2002. Relative motions of Africa, Iberia and Europe during Alpine orogeny. Tectonophysics 359 (1–2), 117–129. https://doi.org/10.1016/S0040-1951(02)00442-0.

Ruiz, M., Diaz, J., Canari, A., Ortuño, M., Vergés, J., 2023. Seismic activity at the eastern Pyrenean termination. Tectonophysics 862, 229977. https://doi.org/10.1016/j.tecto.2023.229977.

Ruiz-Constán, A., Galindo-Zaldívar, J., Pedrera, A., Celerier, B., Marín-Lechado, C., 2011. Stress distribution at the transition from subduction to continental collision (northwestern and central Betic Cordillera). Geochem. Geophys. Geosyst. 12 (12), Q12002. https://doi.org/10.1029/2011GC003824.

Ruiz-Constán, A., Stich, D., Galindo-Zaldívar, J., Morales, J., 2009. Is the northwestern Betic Cordillera mountain front active in the context of the convergent Eurasia-Africa plate boundary? Terra Nova 21 (5), 352–359. https://doi.org/10.1111/j.1365-3121.2009.00886.x.

Sallarès, V., Gailler, A., Gutscher, M.A., Graindorge, D., Bartolomé, R., Gracia, E., Díaz, J., Danobeitia, J.J., Zitellini, N., 2011. Seismic evidence for the presence of Jurassic oceanic crust in the central Gulf of Cadiz (SW Iberian margin). Earth Planet. Sci. Lett. 311 (1–2), 112–123. https://doi.org/10.1016/j.epsl.2011.09.003.

Santos-Bueno, N., Fernández-García, C., Stich, D., Mancilla, F.D.L., Martín, R., Molina-Aguilera, A., Morales, J., 2019. Focal mechanisms for subcrustal earthquakes beneath the Gibraltar Arc. Geophys. Res. Lett. 46 (5), 2534–2543. https://doi.org/10.1029/2018GL081587.

Sanz de Galdeano, C., Alfaro, P., 2004. Tectonic significance of the present relief of the Betic Cordillera. Geomorphology 63 (3–4), 175–190. https://doi.org/10.1016/j.geomorph.2004.04.002.

Sanz de Galdeano, C., García Tortosa, F.J., Peláez Montilla, J.A., Alfaro García, P., Azañón, J.M., Galindo Zaldívar, J., López-Casado, C., López-Garrido, A.C., Rodríguez-Fernández, J., Ruano, P., 2012. Main active faults in the Granada and Guadix-Baza basins (Betic Cordillera). J. Iberian Geol. 38 (1), 209–223. https://doi.org/10.5209/rev_JIGE.2012.v38.n1.39215.

Schettino, A., Turco, E., 2011. Tectonic history of the western Tethys since the Late Triassic. Geol. Soc. Am. Bull. 123 (1–2), 89–105. https://doi.org/10.1130/B30064.1.

Schmid, S.M., Fügenschuh, B., Kissling, E., Schuster, R., 2004. Tectonic map and overall architecture of the Alpine orogen. Eclogae Geol. Helv. 97, 93–117. https://doi.org/10.1007/s00015-004-1113-x.

Scotti, V.N., Molin, P., Faccenna, C., Soligo, M., Casas-Sainz, A., 2014. The influence of surface and tectonic processes on landscape evolution of the Iberian Chain (Spain): quantitative geomorphological analysis and geochronology. Geomorphology 206, 37–57. https://doi.org/10.1016/j.geomorph.2013.09.017.

Serpelloni, E., Vannucci, G., Pondrelli, S., Argnani, A., Casula, G., Anzidei, M., Baldi, P., Gasperini, P., 2007. Kinematics of the Western Africa-Eurasia plate boundary from focal mechanisms and GPS data. Geophys. J. Int. 169 (3), 1180–1200. https://doi.org/10.1111/j.1365-246X.2007.03367.x.

Shen, Z.K., Wang, M., Zeng, Y., Wang, F., 2015. Optimal interpolation of spatially discretized geodetic data. Bull. Seismol. Soc. Am. 105 (4), 2117–2127. https://doi.org/10.1785/0120140247.

Silva, P.G., Goy, J.L., Somoza, L., Zazo, C., Bardají, T., 1993. Landscape response to strike-slip faulting linked to collisional settings: quaternary tectonics and basin formation in the Eastern Betics, southeastern Spain. Tectonophysics 224 (4), 289–303. https://doi.org/10.1016/0040-1951(93)90034-H.

Simón, J.L., 1982. Compresión y distensión alpinas en la Cadena Ibérica Oriental. University of Zaragoza, p. 255 (Ph.D. thesis).

Skikra, H., Lanari, R., Soulaimani, A., Ouabid, M., Raji, O., Amrouch, K., 2025. Spatiotemporal evolution of tectonic stresses during the High Atlas Cenozoic basin inversion: impact of plate kinematics and structural inheritance. Tectonics 44 (3), e2024TC008618. https://doi.org/10.1029/2024TC008618.

Sparacino, F., Palano, M., Peláez, J.A., Fernández, J., 2020. Geodetic deformation versus seismic crustal moment-rates: insights from the Ibero-Maghrebian region. Remote Sens. 12 (6), 952. https://doi.org/10.3390/rs12060952.

Srivastava, S.P., Roest, W.R., Kovacs, L.C., Oakey, G., Levesque, S., Verhoef, J., Macnab, R., 1990. Motion of Iberia since the late Jurassic: results from detailed aeromagnetic measurements in the Newfoundland Basin. Tectonophysics 184 (3–4), 229–260. https://doi.org/10.1016/0040-1951(90)90442-B.

Stich, D., Batlló, J., Macià, R., Teves-Costa, P., Morales, J., 2005. Moment tensor inversion with single-component historical seismograms: the 1909 Benavente (Portugal) and Lambesc (France) earthquakes. Geophys. J. Int. 162 (3), 850–858. https://doi.org/10.1111/j.1365-246X.2005.02680.x.

Stich, D., Mancilla, F.D.L., Pondrelli, S., Morales, J., 2007. Source analysis of the February 12th 2007, Mw 6.0 Horseshoe earthquake: implications for the 1755 Lisbon earthquake. Geophys. Res. Lett. 34 (12), L12308. https://doi.org/10.1029/2007GL030012.

Stich, D., Serpelloni, E., de Lis Mancilla, F., Morales, J., 2006. Kinematics of the Iberia-Maghreb plate contact from seismic moment tensors and GPS observations. Tectonophysics 426 (3–4), 295–317. https://doi.org/10.1016/j.tecto.2006.08.004.

Stucchi, M., Rovida, A., Gómez Capera, A.A., Alexandre, P., Camelbeeck, T., Demircioglu, M.B., Gasperini, P., Kouskouna, V., Musson, R.M.W., Radulian, M., Sesetyan, K., Vilanova, S., Baumont, D., Bungum, H., Fäh, D., Lenhardt, W., Makropoulos, K., Martínez-Solares, J.M., Scotti, O., Živčić, M., Albini, P., Batllo, J., Papaioannou, C., Tatevossian, R., Locati, M., Meletti, C., Giardini, D., 2013. The SHARE European earthquake catalogue (SHEEC) 1000-1899. J. Seismol. 17, 523–544. https://doi.org/10.1007/s10950-012-9335-2.

Styron, R., Pagani, M., 2020. The GEM global active faults database. Earthq. Spectra 36 (1), 160–180. https://doi.org/10.1177/8755293020944182.

Teixell, A., Ayarza, P., Zeyen, H., Fernandez, M., Arboleya, M.L., 2005. Effects of mantle upwelling in a compressional setting: the Atlas Mountains of Morocco. Terra Nova 17 (5), 456–461. https://doi.org/10.1111/j.1365-3121.2005.00633.x.

Teixell, A., Labaume, P., Ayarza, P., Espurt, N., de Saint Blanquat, M., Lagabrielle, Y., 2018. Crustal structure and evolution of the Pyrenean-Cantabrian belt: a review and new interpretations from recent concepts and data. Tectonophysics 724, 146–170. https://doi.org/10.1016/j.tecto.2018.01.009.

Tendero-Salmerón, V., Ercilla, G., González-Castillo, L., Madarieta-Txurruka, A., Martínez-Moreno, F.J., Estrada, F., Galindo-Zaldívar, J., 2024. Gravimetric survey and modelling of a tectonic indenter boundary: the Palomares Fault Zone (Betic Cordillera, Iberia). Tectonophysics 872, 230147. https://doi.org/10.1016/j.tecto.2023.230147.

Tendero-Salmerón, V., Galindo-Zaldívar, J., Pelaez, J.A., Martínez-Martos, M., Henares, J., Marín-Lechado, C., Gil, A.J., López-Garrido, Á.C., 2020. Seismicity in strike-slip foreland faults (central Betic cordillera front): evidence of indentation tectonics. Tectonics 39 (7), e2020TC006143. https://doi.org/10.1029/2020TC006143.

Thinon, I., Matias, L., Réhault, J.P., Hirn, A., Fidalgo-González, L., Avedik, F., 2003. Deep structure of the Armorican Basin (Bay of Biscay): a review of Norgasis seismic reflection and refraction data. J. Geol. Soc. 160 (1), 99–116. https://doi.org/10.1144/0016-764901-103.

Tortella, D., Torné, M., Pérez-Estaún, A., 1997. Geodynamic evolution of the eastern segment of the Azores-Gibraltar zone: the Gorringe Bank and the Gulf of Cadiz region. Mar. Geophys. Res. 19, 211–230. https://doi.org/10.1023/A:1004258510797.

Townend, J., Zoback, M.D., 2006. Stress, strain, and mountain building in central Japan. J. Geophys. Res. Solid Earth 111 (B3), B03411. https://doi.org/10.1029/2005JB003759.

Udías, A., Buforn, E., de Gauna, J.R., 1989. In: Catalogue of Focal Mechanisms of European Earthquakes. Universidad Complutense de Madrid, Department de Geofísica, p. 274.

van Hinsbergen, D.J.J., Vissers, R.L.M., Spakman, W., 2014. Origin and consequences of western Mediterranean subduction, rollback, and slab segmentation. Tectonics 33 (4), 393–419. https://doi.org/10.1002/2013TC003349.

Vannucci, G., Gasperini, P., 2004. The new release of the database of Earthquake Mechanisms of the Mediterranean Area (EMMA Version 2). Ann. Geophys. 47 (1), 307–334. https://hdl.handle.net/11585/19002.

Vavryčuk, V., 2014. Iterative joint inversion for stress and fault orientations from focal mechanisms. Geophys. J. Int. 199 (1), 69–77. https://doi.org/10.1093/gji/ggu224.

Vergés, J., Fernàndez, M., 2006. Ranges and basins in the Iberian Peninsula: their contribution to the present topography. Geol. Soc. Lond. Mem. 32 (1), 223–234. https://doi.org/10.1144/GSL.MEM.2006.032.01.13.

Villamor, P., Capote, R., Stirling, M.W., Tsige, M., Berryman, K.R., Martínez-Díaz, J.J., Martín-González, F., 2012. Contribution of active faults in the intraplate area of

Iberia to seismic hazard: the Alentejo-Plasencia Fault. J. Iberian Geol. 38 (1), 81–111. https://doi.org/10.5209/rev_JIGE.2012.v38.n1.39207.

Villani, F., Antonioli, A., Pastori, M., Baccheschi, P., Ciaccio, M.G., 2024. Stress patterns and crustal anisotropy in the Eastern Alps: insights from seismological and geological observations. Tectonics 43 (3), e2023TC008033. https://doi.org/10.1029/2023TC008033.

Vissers, R.L.M., Meijer, P.T., 2012. Iberian plate kinematics and Alpine collision in the Pyrenees. Earth-Sci. Rev. 114 (1–2), 61–83. https://doi.org/10.1016/j.earscirev.2012.05.001.

Zitellini, N., Gràcia, E., Matias, L., Terrinha, P., Abreu, M.A., DeAlteriis, G., Henriet, J.P., Danobeitia, J.J., Masson, D.G., Mulder, T., Ramella, R., Somoza, L., Diez, S., 2009. The quest for the Africa-Eurasia plate boundary west of the Strait of Gibraltar. Earth Planet. Sci. Lett. 280 (1–4), 13–50. https://doi.org/10.1016/j.epsl.2008.12.005.

Zitellini, N., Rovere, M., Terrinha, P., Chierici, F., Matias, L., BIGSETS Team, 2004. Neogene through Quaternary tectonic reactivation of SW Iberian passive margin. Pure Appl. Geophys. 161, 565–587. https://doi.org/10.1007/s00024-003-2463-4.

Zoback, M.D., Zoback, M.L., Mount, V.S., Suppe, J., Eaton, J.P., Healy, J.H., Oppenheimer, D., Reasenberg, P., Jones, L., Raleigh, C.B., Wong, I.G., Wentworth, C., 1987. New evidence on the state of stress of the San Andreas fault system. Science 238 (4830), 1105–1111. https://doi.org/10.1126/science.238.4830.1105.

Zoback, M.L., Zoback, M., 1980. State of stress in the conterminous United States. J. Geophys. Res. Solid Earth 85 (B11), 6113–6156. https://doi.org/10.1029/JB085iB11p06113.